IMAGE: A MAP OF THE STARS OF THE ORION CONSTELLATION

Print ISSN: 2631-8474 Online ISSN: 2631-8482

JournalPreview

London Journal of Engineering Research

Volume 22 | Issue 9 | Compilation 1.0

London Journals Press

WWW.JOURNALSPRESS.COM

JournalPreview

LONDON JOURNAL ENGINEERING RESEARCH

Journal Content
In this Issue

London Journals Press

i. Journal introduction and copyrights
ii. Featured blogs and online content
iii. Journal content
iv. Editorial Board Members

1. A Study on the Effect of Whitening, Wrinkle Improvement, and Trans-2-Nonenal Removal of Wheat Germ Hydrothermal Extract. ***1-12***
2. Comparisons Between Distributed Power Flow Controller (DPFC) and Unified Power Flow Controller (UPFC). ***13-24***
3. Relationship between Asphalt Concrete Linear Stress Limit and Bitumen Shear Stress Limit. ***25-34***
4. The Generators Created by Ferranti and Hasselwander, a Subject to Study to Save on Current Electrical Energy Production. ***35-42***

V. London Journals Press Memberships

A Study on the Effect of Whitening, Wrinkle Improvement, and Trans-2-Nonenal Removal of Wheat Germ Hydrothermal Extract

Xu Jing, Yuri Kang, Jiyoung Shin & Woonjung Kim

University of Hannam

ABSTRACT

Herein, we investigated the active ingredients in wheat germ as natural materials for functional cosmetics. Wheat germ hydrothermal extracts were obtained with 20 %, 50 %, and 80 % ethanol and used for GC-MS active ingredient analysis and antioxidant efficacy, whitening, wrinkle improvement, and trans-2-nonenal reduction rate analyses. Chromaticity analysis showed a rapid decrease in yellowness (b*), which was believed to be attributed to the increased level of active substances having double bonds with increased ethanol content. GC-MS analysis identified high levels of hexadecanoic acid, 9, 12-octadecadienoic acid, and conjugated linoleic acid with increasing ethanol content. Also, low levels of linoleic acid ethyl ester and linoelaidic acid were detected. In contrast, as the ethanol content decreased, the active ingredients of cyclotrisiloxane were seen.

Keywords: wheat germ, hydrothermal extract, skin whitening, anti-wrinkle, tyrosinase, collagenase, trans-2-nonenal.

Classification: DDC Code: 813.4 LCC Code: PS2472

Language: English

London Journals Press

LJP Copyright ID: 392951
Print ISSN: 2631-8474
Online ISSN: 2631-8482

London Journal of Engineering Research

Volume 22 | Issue 9 | Compilation 1.0

A Study on the Effect of Whitening, Wrinkle Improvement, and Trans-2-Nonenal Removal of Wheat Germ Hydrothermal Extract

Xu Jing[α], Yuri Kang[σ], Jiyoung Shin[ρ] & Woonjung Kim[Ↄ]

ABSTRACT

Herein, we investigated the active ingredients in wheat germ as natural materials for functional cosmetics. Wheat germ hydrothermal extracts were obtained with 20 %, 50 %, and 80 % ethanol and used for GC-MS active ingredient analysis and antioxidant efficacy, whitening, wrinkle improvement, and trans-2-nonenal reduction rate analyses. Chromaticity analysis showed a rapid decrease in yellowness (b), which was believed to be attributed to the increased level of active substances having double bonds with increased ethanol content. GC-MS analysis identified high levels of hexadecanoic acid, 9, 12-octadecadienoic acid, and conjugated linoleic acid with increasing ethanol content. Also, low levels of linoleic acid ethyl ester and linoelaidic acid were detected. In contrast, as the ethanol content decreased, the active ingredients of cyclotrisiloxane were seen.*

Antioxidant efficacy analysis showed an IC_{50} value of 2.16 for ascorbic acid, which was the control, and 3.37, 3.39, and 2.76 for wheat germ extract with 20 %, 50 %, and 80 % ethanol, respectively.

All extracts displayed concentration-dependent antioxidant effects, although the effects were lower than that of ascorbic acid. Tyrosinase inhibition activity analysis showed that the extract with 80 % ethanol had the highest inhibition rate.

In collagenase inhibition activity analysis, all extracts had a similar level of inhibitory activity compared with ascorbic acid. These effects are thought to be attributed to the active ingredients of cyclotrisiloxane detected in the extract.

Additionally, trans-2-noneal removal analysis using GC-MS showed a high removal rate of 96.3 % in a wheat germ extract with 80 % ethanol.

Keywords: wheat germ, hydrothermal extract, skin whitening, anti-wrinkle, tyrosinase, collagenase, trans-2-nonenal.

Author α σ ρ: Department of Cosmetic Science, University of Hannam, Daejeon, 34430, Korea.
Ↄ: Department of Chemistry, University of Hannam, Daejeon, 34430, Korea.
† Corresponding author (e -mail: wjkim@hnu.kr)

I. INTRODUCTION

Recently, there has been increasing interest in natural ingredients for food products and cosmetics, following the growing idea of naturalism for improved living standards and health. As demand for functional cosmetics is increasing, studies are actively investigating functional ingredients that can minimize the side effects of chemical ingredients on the skin, and natural extracts are being tested for their functional effects[1,2].

During aging, the skin undergoes various changes, including pigmentation and wrinkle formation. It produces melanin pigments to protect the internal and skin cells from ultraviolet (UV) rays.

However, excessive melanin production due to continuous UV exposure causes pigmentation, such as freckles and blemishes, accelerating skin aging. Melanin is first produced as tyrosine in melanocytes, which is oxidized by tyrosinase to become 3, 4-dihydroxy phenylalanine (DOPA).

DOPA is then converted to DOPA quinone, which is converted to melanin after various oxidative polymerization reactions[3]. Skin aging can be

London Journal of Engineering Research

divided into intrinsic aging, caused by physiological aging, and extrinsic aging, caused by continuous UV exposure. Photoaging caused by UV exposure is considered the primary cause of skin aging [4]. Following skin aging, the production of structural proteins of the skin, such as collagen and elastin, is reduced, and collagenase biosynthesis is increased. This leads to greater expression of matrix metalloproteinases (MMPs), inducing matrix protein degradation in the dermis that deteriorates skin elasticity and results in skin sagging and wrinkles[5]. Additionally, impaired metabolism, along with skin aging, accumulates waste in the skin layers. As monounsaturated fatty acids in the skin surface lipids are decomposed, substances including nonenal aldehyde with a peculiar smell that are often observed in the elderly are generated [6,7]. 2-Nonenal is a long-chain aliphatic aldehyde containing nine carbons and unsaturated bonds. It is the primary cause of age-related, unpleasant, greasy, and sweaty odors and is found from age 40 onwards [8,9]. With aging, elderlies in their 60s and 70s have a slower, impaired olfactory function and fail to be aware of their scent. In particular, elderlies in their 60s and 70s have reduced absolute and relative sensitivity to smells, approximately 100 times lower than people in their 20s and 30s.[10].

According to the South Korea Ministry of Food and Drug Safety, products for skin whitening and wrinkle improvement are considered functional cosmetics. There are nine whitening materials registered with the Ministry of Food and Drug Safety, including arbutin, niacinamide, ascorbyl glucoside, mulberry extract, liquorice extract, and ethyl ascorbyl ether, and four types of raw materials, including adenosine, retinol, and polyethoxylated-retinide, which are known for wrinkle improvement effects [11]. However, there is still a lack of functional raw materials. Therefore, further studies must investigate functional materials for natural cosmetics that contain active ingredients for the skin while reducing the side effects caused by synthetic raw materials [12].

Additionally, studies on natural extracts are expected to induce technological and industrial growth. As there are sufficient demands for industrial development and consumer preference, the natural extracts must have competitive efficacy, safety, stability, and cost [13].

Wheat germ is produced as a by-product during the milling process of wheat. Pure wheat germ can be isolated for production due to its low cost and adequate demand and supply. Previous studies on germs of various grains, other than wheat, showed that polyphenols in barley germ have antioxidant effects [14,15]. Similarly, rice germs increased the protein content and enhanced the physiological activity through microbial fermentation[16]. Rice bran, a by-product of rice, lowered blood cholesterol level [17], and arabinoxylan extracted from rice bran inhibited cancer cell toxicity of natural killer (NK) cells [18]. Germs of Keunnunjami, a new rice variety, also have antioxidant effects [19,20].

Studies on wheat germ reported its anti- bacterial [21], anti-inflammatory [22], antioxidant [23], and immune-enhancing [24] effects. The wheat germ fat contains a high level of tocopherol, which makes it a valuable, healthy, functional food [25].

However, most studies on wheat germ focused on food materials, and there is a lack of studies on wheat germ as a cosmetic raw material. Therefore, this study aimed to analyze the antioxidant, whitening, wrinkle improvement, and trans-2-nonenal reduction effects of wheat germ hydrothermal extract through chromaticity analysis and GC-MS active ingredient analysis to confirm its functionality as a cosmetic material.

II. EXPERIMENT

2.1 Material

The wheat germ used in this study was provided by DAEHAN FLOUR MILLS CO., LTD., in November 2021.

2.2 Wheat Germ Extraction Condition

Wheat germ powder was used for the hydrothermal extraction of wheat germ. Water and ethanol were used as the solvent, and hydrothermal extraction was conducted with 20 %, 50 %, and 80 % ethanol. The total volume of the solvent was 300 ml, which was mixed with 30

g of wheat germ. A high-pressure hydrothermal extractor (KSP-240L, KYUNGSEO E&P, Inch eon, Korea) was used at 80 °C and 0.06 MPa for 3 h extraction. The extracted solution was decompression-filtered (DOA-P704-AC, G AST Manufacturing Inc., U.S.A) using a 90 mm filter (20 HM Hyundai Micro, Korea) and decompression-concentrated (EYELA N-1300, SHANGHAI EYE LA CO., China) for storage at 4 ℃.

The weight of the extracted sample after filtration under reduced pressure containing ethanol and the weight after concentration by completely evaporating the ethanol was used to calculate the extract yield (%) as follows.

$$Extract\ yield\ (\%) = \frac{Weight\ after\ concentration}{Weight\ after\ decompression} \times 100$$

2.3 Chromaticity Analysis of Wheat Germ Extract

The wheat germ extracts with varying ethanol contents analyses using a colorimeter (CR-400, Konica Minolta, Tokyo, Japan) was repeated three times, and the mean value was calculated. The value was expressed as L*(brightness), a*(redness), and b*(yellowness).

2.4 GC-MS Analysis of Wheat Germ Extract

GC-MS (Gas chromatography-mass spectrometry) was performed to analyze the active ingredients of wheat germ extract. HP-5ms (30 m x 250 μm x 0.25 μm) column (Agilent 19091S-433UI: 1456957H, Agilent technology, U.S.A) HP-5ms (30 m x 250 μm x 0.25 μm) was used for GC analysis. The carrier gas was helium, and the pressure and flow rate were set to 7.0699 psi and 1 mL/min, respectively. The temperature range of the column was –60–325 °C, and the oven temperature was 40–300 °C. GC-MS was conducted for a total of 45 min.

2.5 DPPH Scavenging Activity Analysis of Wheat Germ Extract

DPPH scavenging activity was measured using 95 % powder DPPH standard sample 2,2-Diphenyl-1-picrylhydrazyl (Alfa Aesar, Massachusetts, USA) (free radical) to assess the antioxidant effects of wheat germ extract. After diluting 5 g of all extracts with an ethanol content of 20 %, 50 %, and 80 % in 100 ml ethanol, the solution was re-diluted in ethanol at varying concentrations of 5 %, 10 %, 15%, 20 %, and 30%.

Then, 1.5 mM DPPH solution dissolved in methanol, wheat germ extract diluted at different concentrations, and ethanol were mixed in a ratio of 6 (600 μl): 3 (300 μl): 1 (100 μl) and reacted for 20 min in the absence of light. Absorbance was measured at 517 nm with a UV/Vis Spectrophotometer (KLAB, Deajeon, Korea).

Ascorbic acid was used as the control substance, and 0.1 mg/ml of ascorbic acid was mixed in an identical ethanol ratio to the wheat germ extract for identical testing conditions. The inhibition rate of DPPH Radical scavenging activity, indicated as IC50, was calculated as follows.

$$Inhibition\ rate\ (\%) = \frac{Abs\ (control) - Abs\ (sample)}{Abs(control)}$$

$$\mathrm{bs_{sample}} = \mathrm{Abs_{test}} - \mathrm{Abs_{color}}$$

2.6 Analysis of Tyrosinase Inhibition Rate by Wheat Germ Extract

The tyrosinase inhibition activity on the whitening effect of wheat germ extract was evaluated. A substrate solution (0.2 ml), 0.02 g of 10 mM L-DOPA (3,4-Dihydroxy-L-phenylalanine, Sigma Aldrich, St. Louis, USA), 0.4 ml of the buffer, 0.2 ml of wheat germ extract, and 125 U/ml 0.2 ml of enzyme mushroom tyrosinase (T3824-25KU, Sigma Aldrich, St. Louis, USA) were added to 10 ml of 67 mM sodium phosphate buffer (pH 6.8).

The mix was stirred and reacted at 25 ℃ for 30 min. After centrifugation, the supernatant was

transferred to a quartz cuvette (Quartz Cell, KMS, Korea). The absorbance of DOPA Chrome produced in the reaction solution was measured at 475 nm using a UV/Vis Spectrophotometer.

Kojic acid was used as a positive control. A total of 0.002 g of Kojic acid was added to 10 ml of DW, and the same experiment was performed. The control group without wheat germ extract and the experimental group with wheat germ extract were compared to calculate the tyrosinase inhibition rate.

$$Inhibtion\ rate\ (\%) = \frac{Extract\ sample\ O.D}{Control\ group\ O.D} \times 100$$

2.7 Analysis of Collagenase Inhibition Rate by Wheat Germ Extract

Collagenase inhibition activity dependence on wheat germ extract was analyzed as follows. A mixture of 0.1 M tris and 4 mM CaCl2 was mixed with buffer (pH 7.5) with 1 M HCl, 0.25 ml of 1.2 mg/ml 4-phenylazo benzyloxycarbonyl Pro-Leu-Gly-Pro-D-Arg (Sigma Aldrich, St. Louis, MO, USA) substrate solution, 0.1 ml of wheat germ extract, and 0.15 ml of buffer with 0.4 mg/ml of collagenase (CD130-100MG, Sigma Aldrich, St. Louis, U.S.A). The final mixture was reacted at 37 ℃ for 30 min and mixed with 0.5 ml of 20 % citric acid diluted with DW and 2.4 ml of ethyl acetate to terminate the reaction. After stirring and centrifugation at 120 RPM for 10 min (HA-12, Hanil Industrial, Incheon, Korea), the supernatant was transferred to a quartz cuvette, and the absorbance was measured at 320 nm using a UV/Vis Spectrophotometer. Ascorbic acid at a concentration of 0.1 g/ml was used as a positive control, and an identical experiment was performed.

The control group without wheat germ extract and the experimental group with wheat germ extract were used to calculate the collagenase inhibition rate with the following formula.

$$Inhibtion\ rate\ (\%) = \frac{Extract\ sample\ O.D}{Control\ group\ O.D} \times 100$$

2.8. Analysis of trans-2-nonenal reaction rate by wheat germ extract using GC-MS

A reference solution was prepared using 100 ml of ethanol and 9 μl of Trans-2-Nonenal (TOKYO CHEMICAL INDUSTRY, Tokyo, Japan). Then, 1000 ul of the reference solution was mixed with 6, 6, and 4 ul of wheat germ extract with 20 %, 50 %, and 80 % ethanol, respectively. The mix was centrifuged and dispersed at 500 RPM for 30 min.

Subsequently, 150 ul of Fehling solutions A and B (Daejeong Chemical Co., Ltd., Siheung, Korea) with aldehyde group reducibility were added and incubated in an oven at 60 ℃ for 15 min. The mix was centrifuged, and the supernatant was used for GC analysis (Agilent 123-7063). The oven temperature was maintained at 50 ℃ for 3 min and increased by 5 ℃/min to a final temperature of 240 ℃, which was maintained for 2 min for analysis.

III. RESULTS AND DISCUSSION

The results of this study on wheat germ extract are displayed below. The notations for wheat germ extract with 20 %, 50 %, and 80 % ethanol are A, B, and C, respectively.

3.1 Wheat Germ Extract Yield

As shown in Table 1, the yield of wheat germ extracts according to the extraction conditions tended to decrease rapidly as the ethanol content increased. As ethanol's boiling point is 78 ℃, the set temperature of 80 ℃ during hydrothermal extraction may have been attributed to a decreased yield of wheat germ extract with increasing ethanol content.

Table 1: Yield table for wheat germ extracts

No.	DW:EtOH	Extract	After decompression (g)	After concentration (g)	Yield (%)
A	80 : 20		110	79.4	72.2
B	50 : 50		211	135	64.0
C	20 : 80		172	38.8	22.6

3.2 Colorimetric Measurement of Wheat Germ Extract

Table 2 shows that increasing the ethanol content decreased brightness (L*) while increasing redness (a*) and yellowness (b*). In particular, yellowness tended to grow rapidly, which is thought to be related to the gradual increase in active substances with double bonds, following increased ethanol content.

Table 2: Colorimetric Results for Wheat Germ Extract

No.	A	B	C
			
L^* (brightness)	23.6	20.6	15.1
a^* (redness)	0.95	0.70	0.58
b^* (yellowness)	-0.38	5.55	10.0

3.3 Analysis Result of Wheat Germ Extract Active Ingredients

GC-MS analysis identified various active ingredients as functional cosmetic materials in wheat germ extract. A comparison of wheat germ extract with ethanol content showed low levels of active ingredients in extract A in contrast to high levels of active ingredients detected in extracts B and C. The results are shown in Figures 1–3.

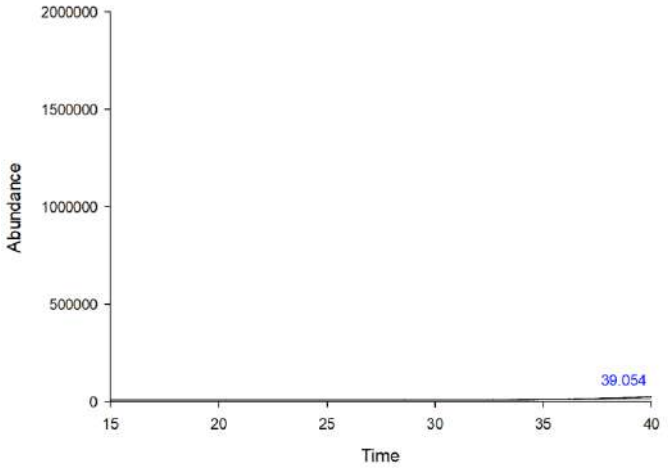

Figure 1: GC-MS Chromatogram of 20% Ethanol Extracts of Wheat Germ

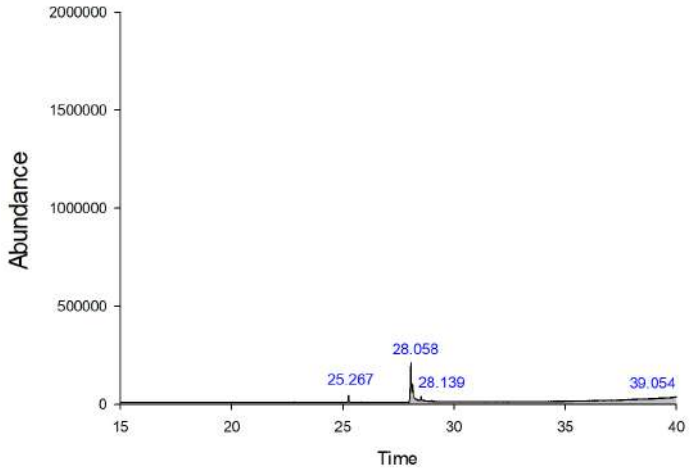

Figure 2: GC-MS Chromatogram of 50% Ethanol Extracts of Wheat Germ

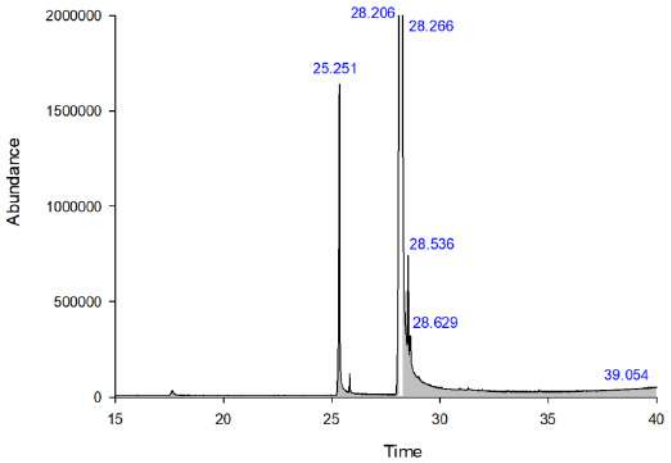

Figure 3: GC-MS Chromatogram of 80% Ethanol Extracts of Wheat Germ

As shown in Tables 3–5, extracts with higher ethanol content were associated with more active ingredients. In particular, in extract A, cyclotrisiloxane, an antibacterial and antioxidant active ingredient, was detected. In extract B, hexadecanoic acid, conjugated linoleic acid, and 9, 12-octadecadienoic acid with antioxidant effects were detected. In extract C, in addition to hexadecanoic acid, conjugated linoleic acid, and 9, 12-octadecadienoic acid, linoleic acid ethyl ester, and linoelaidic acid were also identified.

Table 3: GC-MS chromatogram profile of 20% ethanol of wheat germ

Retention time (RT)	Name of the compound	Quality	Area peak (%)
39.054	Cyclotrisiloxane	47	17.0

Table 4: GC-MS Chromatogram Profile of 50% Ethanol of Wheat Germ

Retention time (RT)	Name of the compound	Quality	Area peak (%)
25.267	Hexadecanoic acid	99	7.84
28.058	9,12-Octadecadienoic acid	99	53.3
28.139	Conjugated linoleic acid	95	38.8
39.054	Cyclotrisiloxane	47	18.0

Table 5: GC-MS Chromatogram Profile of 80% Ethanol of Wheat Germ

Retention time (RT)	Name of the compound	Quality	Area peak (%)
25.251	Hexadecanoic acid	99	8.33
28.206	9,12-Octadecadienoic acid	99	57.7
28.266	Conjugated linoleic acid	99	27.5
28.536	Linoleic acid ethyl ester	99	3.34
28.629	Linoelaidic acid	97	2.71
39.054	Cyclotrisiloxane	47	19.0

3.4 Analysis Result of Wheat Germ Extract Antioxidant Efficacy

Antioxidation analysis using DPPH was based on the property that 1.1-diphenyl-2-picrylhydrazyl (DPPH) is a relatively stable free radical with an absorption band at 517 nm. DPPH, in purple, is reduced and discolored to yellow when it encounters electrons or hydrogen radicals from substances with antioxidant effects, and the absorbance of the reduced value was measured26]. DPPH radical scavenging activity of wheat germ extract was assessed. Ascorbic acid in the control group had an IC50 of 2.16. In extracts A, B, and C, IC50 was 3.37, 3.39, and 2.76, respectively. Thus, all samples showed antioxidant effects in a concentration-dependent manner (Figure 4), although the effects were lower than that of control ascorbic acid. In particular, extract C showed more excellent antioxidant effects, which may be attributed to the high levels of antioxidant active ingredients in extract C compared with extracts A and B.

Table 6: Half maximal inhibitory concentration (IC50)

No.	IC_{50}
Ascorbic acid	2.16
A	3.37
B	3.39
C	2.76

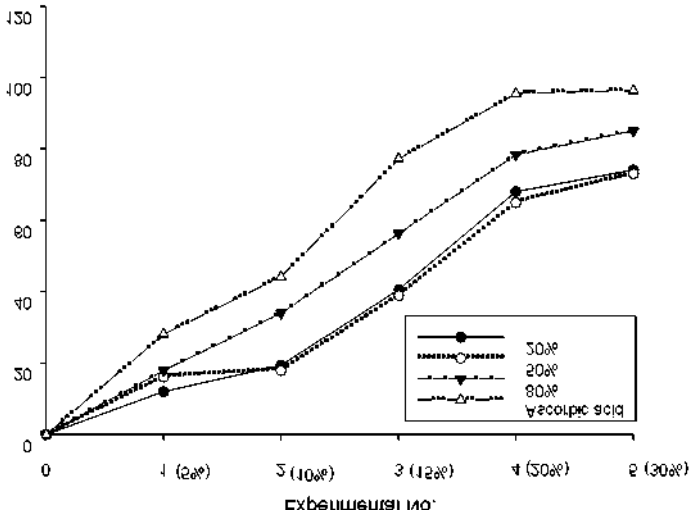

Figure 4: Antioxidant ability according to extraction conditions

3.5 Analysis Result of Tyrosinase Inhibitory Activity by Wheat Germ Extract

Figure 5 shows tyrosinase inhibition activity for each wheat germ extract. As the ethanol content increased, the tyrosinase inhibition rate increased. In particular, extract C with 80 % ethanol showed an inhibition rate greater than 80 %, suggesting more excellent whitening effects compared with that of the control Kojic acid. The effects are thought to be mediated by the 9, 12-octadecadienoic acid, linoleic acid ethyl ester, linoelaidic acid, and conjugated linoleic acid.

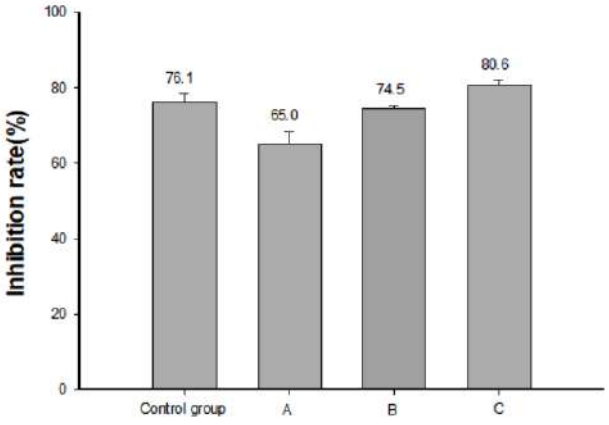

Figure 5: Effect of wheat germ extracts on tyrosinase inhibitory activity

3.6 Analysis Result of Collagenase Inhibitory Activity by Wheat Germ Extract

Collagen does not react to proteolytic enzymes; however, studies reported that collagen is degraded by collagenase. Reduced collagenase activity is essential in lowering skin elasticity, therefore suppressing wrinkle formation. Wrinkle improvement by wheat germ extract is shown in Figure 6. All extracts showed a similar collagenase inhibition rate as ascorbic acid. It is thought that the active ingredient, cyclotrisioloxane, identified in GC-MS component analysis, mediates these effects.

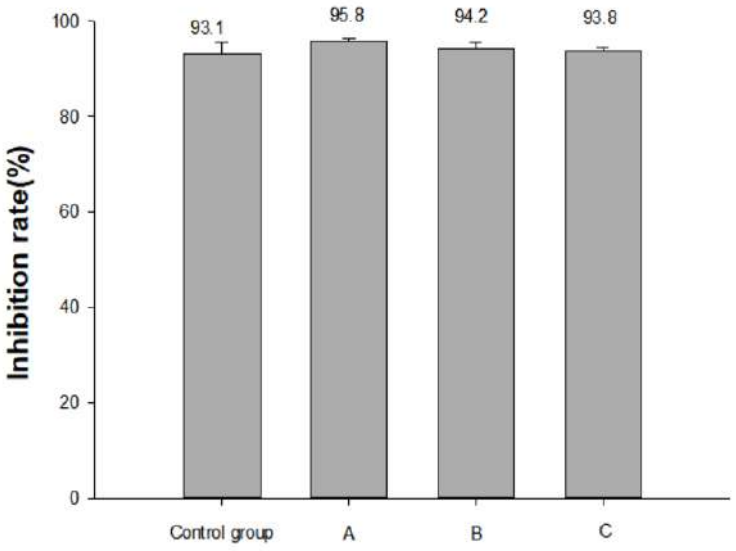

Figure 6: Effect of Wheat Germ Extracts on Collagenase Inhibitory Activity

3.7 Analysis Result of Trans-2-Nonenal Removal by Wheat Germ Extract Using GC-MS

Table 7 and Figure 7 show the overall removal rate of trans-2-nonenal analyzed using GC-MS. The removal rate was 83.5 % in extract A, 94.9 % in extract B, and 96.3 % in extract C, which indicated high trans-2-nonenal removal effects by wheat germ extract. This is thought to be attributed to the high levels of active ingredients, 9, 12-octadecadienoic acid, and conjugated linoleic acid, identified in the extract.

Table 7: GC-MS Results for the Evaluation of Trans-2-Nonenal Removal Efficacy of Extracts by Extraction Conditions

	Response	Final conc.	Removal rate(%)
Control	12253		
A	2014	<0.01	83.5
B	613	<0.01	94.9
C	452	<0.01	96.3

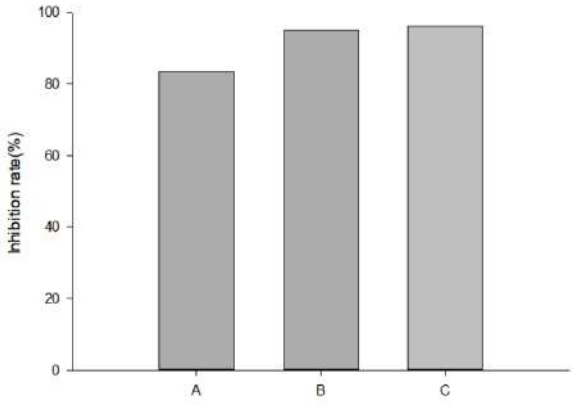

Figure 7: Comparison of GC-MS Results for the Evaluation of Trans-2-Nonenal Removal Efficacy of Extracts According to Extraction Conditions

IV. CONCLUSION

The results of wheat germ hydrothermal extract by ethanol content were as follows:

1. Chromaticity analysis showed decreased brightness (L*) and increased redness (a*) and yellowness (b*). In particular, yellowness tended to increase rapidly, which is thought to be related to the increasing level of effective active ingredients with double bonds as the ethanol level increased.
2. Qualitative analysis of GC-MS indicator components of wheat germ extract showed that as ethanol content increased, the active ingredient increased and was detected at high levels. In extract A, only a low level of the active ingredient of cyclotrisiloxane was detected. In contrast, in extracts B and C, high levels of active ingredients, such as hexadecanoic acid, conjugated linoleic acid, and 9,12-Octadecadienoic acid, were detected.
3. DPPH radical scavenging activity of wheat germ extracts were as follows: IC50 of ascorbic acid, extract A, extract B, and extract C were 2.16, 3.37, 3.39, and 2.76, respectively. All extract samples had lower DPPH radical scavenging activity than ascorbic acid; however, the extract showed concentration-dependent antioxidant effects.
4. Tyrosinase inhibition activity of wheat germ extract increased with ethanol content. In particular, extract C showed a high tyrosinase inhibition rate more excellent than 80 %, suggesting it had greater whitening effects than control Kojic acid. The effects are thought to be mediated by the 9, 12-octadecadienoic acid, linoleic acid ethyl ester, linoelaidic acid, and conjugated linoleic acid.
5. In all extracts, collagenase inhibition activity was similar compared with that in ascorbic acid. This may be attributed to the active ingredient, Cyclotrisiloxane, identified in the extract.
6. Analysis of trans-2-nonenal removal rate by wheat germ extract using GC-MS showed a rate of 83.5 %, 94.9 %, and 96.3 % in extracts A, B, and C, respectively, suggesting a high trans-2-noneal removal rate. The effects are thought to be mediated by the 9, 12-octadecadienoic acid, linoleic acid ethyl ester, linoelaidic acid, and conjugated linoleic acid.

Herein, our findings demonstrated that wheat germ hydrothermal extract contains natural active ingredients for functional skin cosmetics. Wheat germ extract effectively removed trans-2-nonenal, the critical cause of unpleasant odor in the elderly, whilst whitening the skin and improving wrinkles. Therefore, wheat germ extract can be potentially used as a natural material for functional cosmetics.

Acknowledgement

This work is supported by the National Research Foundation of Korea (NRF-2020R1F1A1 074571)

and the 2022 HANNAM University Innovation Research Program.

REFERENCES

1. T. H. Youm, H. B. Lim, "Antimicrobial Activities of Organic Extracts from Fruit of Thuja orientalis L", Korean Journal of Medicinal Crop Science., 18(5), pp. 315-322, (2010).
2. K. D. Kim, S. J. Kim, "The Study on the Efficacy of Herbal Plant Extracts by the Part and Solvent Extraction", Journal of the Society of Cosmetic Scientists of Korea., 33(2), pp. 127-135, (2007).
3. W. M. Pak, K. B. W. R. Kim, M. J. Kim, J. H. Park, N. Y. Bae, S. H. Park, D. H. Ahn, "Anti-Melanogenesis and Anti-Wrinkle Effects of Sargassum micracanthum Extracts", Microbiology and Biotechnology Letters., 44(1), pp. 19-25, (2016).
4. N. Y. Kim, "Effect of Antioxidation and Inhibition of Melanogenesis from Scutellaria baicalensis Extract", Korean Journal of Aesthetics Cosmetology., 12(1), pp. 41-47, (2014).
5. K. H. Lee, H. S. Park, I. J. Yoon, Y. B. Shin, Y. C. Baik, D. H. Kooh, S. K. Kim, H. K. Jung, M. O.Sim, H. W. Cho, W. S. Jung, M. S. Kim, "Whitening and Anti-Wrinkle Effects of Tremella Fuciformis Extracts", Korean Journal of Medicinal Crop Science., 24(1), pp. 38-46, (2016).
6. Y. R. Kang, W. J. Kim, "Characterization Natural Chamaecyparis Obtusa Leaf Extract to Remove Senile Body Odor", London Journal of Research in Science., 21(4), pp. 1-14, (2021).
7. S. Haze, Y. Gozu, S. Nakamura, Y. Kohno, K. Sawano, H. Ohta, K. K. Yamazaki, "2-Nonenal Newly Found in Human Body Odor Tends to Increase with Aging", Journal of Investigative Dermatology., 116(4), 520-524, (2001).
8. S. Y. Lee, J. H. Kim, N. T. Nguyen, R. M. Park, S. M. Lee, S. H. Bang, G. C. Jeon, J. W. Lee, S. C. Kim, B. K. Cho, Y. H. Kim, J. H. Min, "Removal of Trans-2-nonenal Using Hen Egg White Lysosomal-Related Enzymes", Molecular Biotechnology., 26(4), pp. 380-386, (2020).
9. S. Y. Lee, J. W. Lee, A. R. Hwang, Y. H. Kim, J. H. Min, "A Specific Nonenal-Binding Peptide, P4 Screened by Phage Display Can Remove Trans-2-Nonenal", Molecular Biotechnology., 62(5), pp. 273-279, (2020).
10. I. H. Kang, B. C. Min, K. J. Jeon, C. J. Kim,"Evalucation of the Odor with Aging", Korean Journal of the Science of Emotion & Sensibility., 5(2), pp. 1-9, (2002).
11. H. J. Shin, H. L. Jeong, D. B. Hwang, D. U. Kim, "Cudrania tricuspidata Root Extract as Whitening and Antiwrinkle Cosmetic Agent", Korea Chemical Engineering Research., 52(6), pp. 701-705. (2014).
12. I. H. Kim, J. H. Lee, "Skin Whitening and Anti-wrinkle Effects of Chambirum (Amaranthus mangostanus)", Asian Journal of Beauty and Cosmetology., 20(1), pp. 21-31, (2022).
13. G.W.Kim, Y. H. Choi, B. L. Kim, Y. U. Kim, R. S. Seong. M. H. Han, G. A. Kim, M. J. Choi, Y. G. Jeong, "Determination of Anti-oxidative and Whitening Effects of Complex Extracts Obtained from Sprout Panax ginseng C.A. Meyer and Cassia nomame (Sieb.) Honda on Skin", Asian Journal of Beauty and Cosmetology., 16(3), pp. 309-320, (2018).
14. H. M. Seog, M. S. Seo, S. R. Kim, Y. K. Park, Y. T. Lee, "Characteristics of Barley Polyphenol Extract (BPE) Separated from Ling By-products", Korean Journal of Food Science and Technology., 34(5), pp. 775-779, (2002).
15. K. Tamagawa, S. Iizuka, S. Fukushima, Y. Endo, Y. Komiyama, "Antioxidative Activity of Polypenol Extracts from Barley Bran", Nippon Shokuhin Kagaku Kogaku Kaishi., 44(7), pp. 512-515, (1997).
16. H. N. Song, Y. R. Lee, "Biological Activities and Quality Characteristics of Rice Germ after Microbial Fermentation", The Korean Journal of Food And Nutrition., 30(1), pp. 59-66, (2017).
17. T. S. Kahlon, R. M. Saunders F. L. Chow M. C. Chiu, A. A. Betschart, "Effect of Rice Bran and Oat Bran on Plasma Cholesterol in Hamsters", Cereal Foods World., 34(9), pp. 768. (1989).
18. M. Ghoneum, "Enhancement of Human Killer Cell Activity by Modified Arabinoxylan from

Rice Bran(MGN-3)", International Journal of Immunotherapy., 14(2), pp. 89-99, (1998).
19. J. E. Liang, J. W. Ma, S. I. Chung, M. Y. Kang, "Phytosterols Content of Keunnunjami Germ and its Antioxidative Effects in Adult Rats", Journal of Nutrition and Health., 53(2), pp. 99-110, (2020).
20. B. S. Choi, K. O. Kang, "Studies on the Analysis of Physiological and Antimicrobial Activity of Wheat Germ", Journal of the East Asian Society of Dietary Life., 19(4), pp. 585-592, (2009).
21. M. H. Kim, S. H. Jo, K. S. Ha, J. H. Song, H. D. Jang, Y. I. Kwon, "Antimicrobial Activities of 1,4-Benzoquinones and Wheat Germ Extract", Journal of Microbiology and Biotechnology., 20(8), pp. 1204-1209, (2010).
22. B. K. Kang, M. J. Kim, D. H. Jeong, K. B. W. R. Kim, N. Y. Bae, J. H. Park, S. H. Park, D. H. Ahn, "Anti-inflammatory Effect of Wheat Germ Oil on Lipopolysaccharide-stimulated RAW 264.7 Cells and Mouse Ear Edema", Microbiology and Biotechnology Letters., 44(3), pp. 236-245, (2016).
23. S. H. Jo, C. Y. Cho, K. S. Ha, E. J. Choi, Y. R. Kang, Y. I. Kwon, "The Antioxidant and Antimicrobial Activities of Extracts of Selected Barley and Wheat Inhabited in Korean Peninsula", Journal of the Korean Society of Food Science and Nutrition., 42(7), pp. 1003-1007, (2013).
24. E. M. Choi ,T. S. Im, H. L. Lee, J. K. Hwang, "Immune Cell Stimulating Activity of Wheat Arabinoxylan", Korean Journal of Food Science and Technology., 34(3), pp. 510-517, (2002).
25. B. S. Choi, K. O. Kang, "Studies on the Analysis of Physiological and Antimicrobial Activity of Wheat Germ", Journal of the East Asian Society of Dietary Life., 19(4), pp. 585-592 (2009).
26. C. D. Porto, Calligaris S, E. Cellotti, M. C. Nicoli, "Antiradical Properties of Commercial Cognacs Assessed by the DPPH Test", Journal of Agricultural and Food Chemistry., 48(9), pp. 4241-4245, (2000).
27. N. H. Grant, H. E. Alburn, "Studies on the Collagenases of Clostridium Histolyticum", Archives of Biochemistry and Biophysics, 82(2), pp. 245-255, (1959).

Comparisons Between Distributed Power Flow Controller (DPFC) and Unified Power Flow Controller (UPFC)

Olatunde A. Adeoye, Samir I. Abood, John H. Fuller & John O. Attia

A & M University

ABSTRACT

The power industries daily compensate for the rising demand for electric power globally by installing new transmission lines or efficiently operating the current ones, thus transmitting more electricity from one specific point to another. However, building new transmission lines is highly challenging due to the high cost and regulations. In addition, the flow of electricity is predominantly along an undesirable path, and its stability is always affected by voltage fluctuation in the transmission lines. An intelligent approach to mitigating this problem is to control the flow of electric power effectively and efficiently in the transmission line system.

Keywords: intelligent approach, flexible alternating current transmission system (FACTS), unified power flow controller (UPFC), distributed power flow controller (DPFC).

Classification: DDC Code: 538.19 LCC Code: TK3351

Language: English

London Journals Press

LJP Copyright ID: 392952
Print ISSN: 2631-8474
Online ISSN: 2631-8482

London Journal of Engineering Research

Volume 22 | Issue 9 | Compilation 1.0

Comparisons Between Distributed Power Flow Controller (DPFC) and Unified Power Flow Controller (UPFC)

Olatunde A. Adeoye[α], Samir I. Abood[σ], John H. Fuller[ρ] & John O. Attia[Ꞷ]

ABSTRACT

The power industries daily compensate for the rising demand for electric power globally by installing new transmission lines or efficiently operating the current ones, thus transmitting more electricity from one specific point to another. However, building new transmission lines is highly challenging due to the high cost and regulations. In addition, the flow of electricity is predominantly along an undesirable path, and its stability is always affected by voltage fluctuation in the transmission lines. An intelligent approach to mitigating this problem is to control the flow of electric power effectively and efficiently in the transmission line system.

This work outlined the basic operational comparison concepts of Flexible Alternating Current Transmission System (FACTS) devices of the Unified Power Flow Controller (UPFC) and the Distributed Power Flow Controller (DPFC) based on their respective active power exchange.

The UPFC incorporates a common dc-link between its shunt and series converters. The DPFC operates without the common D.C-link, splitting the three-phase series converters into many single-phase series distributed converters via the transmission line. The operational comparison between UPFC and DPFC is modeled and simulated in Matlab/Simulink environment to illustrate their control capability in the flow of electric power. The simulation results show the performance enhancement reliability of the DPFC in improving the voltage stability and power transfer capability over the UPFC.

Keywords: intelligent approach, flexible alternating current transmission system (FACTS), unified power flow controller (UPFC), distributed power flow controller (DPFC).

Author α σ ρ Ꞷ: Department of Electrical and Computer Engineering, Prairie View A&M University, Prairie View, United States of America.

I. INTRODUCTION

Recently, FACTS devices have attracted significant attention because they offer unique properties for regulating alternating current (A.C.) transmission, increasing or reducing the power flow in specific lines, and responding almost instantly to the stability crisis. The ever-growing demand for electrical power worldwide has necessitated transporting more electricity from the generating point to the end-users via interconnected transmission lines [1]. However, the natural flow of electricity can result in the overloading or underloading of the transmission lines, affecting the stability and the controllability of power flow with increased variation in line voltage. The power flow control is challenging since the power system is highly complex, having hundreds of buses and transmission links. In addition, power systems comprising generators, transmission links, and power electronics-based FACTS devices are nonlinear and multivariable systems with active properties over various operating conditions [2].

In recent times, significant research studies have been undertaken to improve the control capability of the transmission interconnection system that supplies power from the generating point to the loads and minimizes operational and maintenance costs. The design of the internal controllers of FACTS devices is solely dependent on the traditional linear control methods of classic or Proportionate Integral (P.I.) controllers and

other power flow control techniques of FACTS devices such as Static Synchronous Compensator (STATCOM), Static VAR Compensator (SVC), Static Series Synchronous Compensator (SSSC), and Gate Controlled Series Capacitors are not effective in providing the solution to the problem of nonlinear loads in power grids [1-2]. Mitigating these undesirable conditions requires using FACTS devices of UPFC and DPFC. These FACTS devices operate in power system networks as electric power flow controllers for the system's parameters, such as line impedance, transmission angle, bus voltage, and components of active power and reactive power [2]. The elimination of the common D.C-link and the splitting of the three-phase series converters into several single-phase series distributed converters via the transmission line make the DPFC provide better performance in controlling electric power flow than UPFC. This paper compares detailed analysis performance of FACTS devices of DPFC and UPFC in a Matlab/Simulink environment. This paper's work is structured as follows: Section II explains the FACTS devices of UPFC and DPFC basic concepts. In section III, comparisons between UPFC and DPFC are described. Section IV is the simulation results and discussions of the UPFC and DPFC. The final section states the paper's conclusions.

II. FACTS DEVICES OF UPFC AND DPFC BASIC CONCEPTS

2.1 UPFC Concept

The UPFC concept is one of the third generations in the FACTS family devices [3]. The UPF controls voltage magnitude, phase angle, and active and reactive power flow via the transmission line. It also has the potential to control three parameters of line power flow, such as line impedance, voltage, and phase angle, simultaneously [4]. This device also provides rapid reactive power compensation for high-voltage power transmission systems.

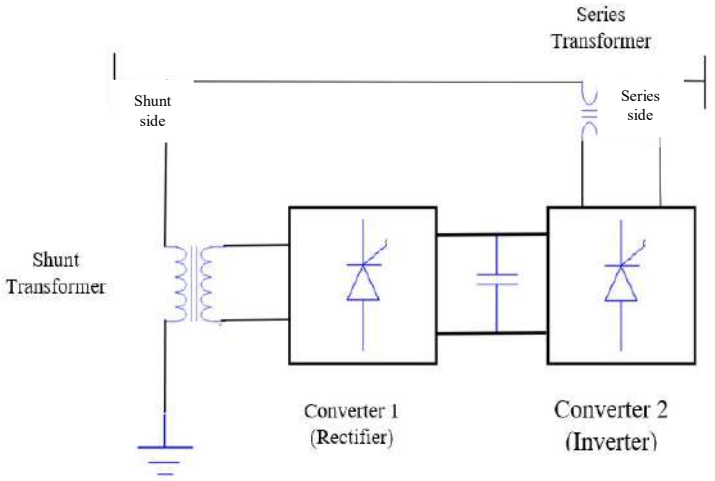

Fig. 1: Basic UPFC Circuit Arrangement

Fig. 1 shows converter 1 (rectifier) and converter 2 (inverter) with a common D.C. link. The UPFC controls the power system transmission line's active and reactive power flows via the series inverter by injecting a symmetrical three-phase voltage of controllable magnitude and phase angle [5]. The inverter operates to transfer the active power to the D.C. terminals. The shunt inverter uses the line D.C positive and negative power to keep the voltage across the storage capacitor constant, thus, making the total active power absorbed by the UPFC from the line equal to the inverters and their respective transformers losses.

Voltage regulation at the point of connection VDC is provided by using the remaining capacity of the shunt inverter to exchange reactive power with the line. The two voltage source inverters can work autonomously by separating the dc side. The shunt inverter operates as a STATCOM (Static

Synchronous Compensator) for generating or absorbing reactive power that regulates the voltage magnitude at the connection point.

Fig. 2 shows the shunt control block diagram in which the shunt controller in UPFC operates to charge the dc-link capacitor voltage that enhances the series converter for improved power flow control and maintaining voltage profile [6].

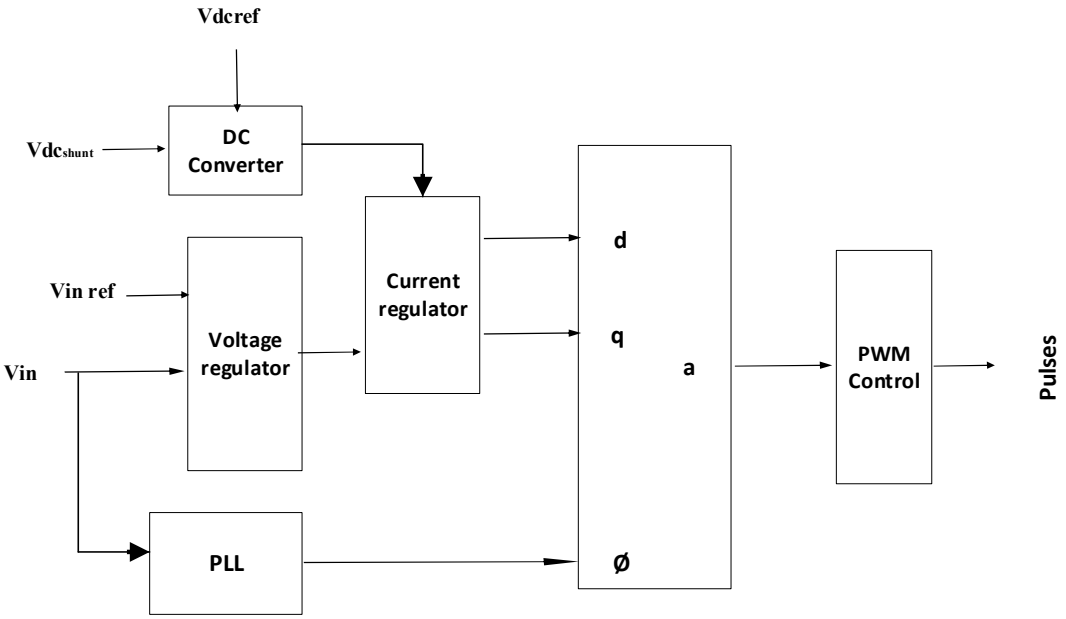

Fig. 2: UPFC shunt control block diagram [6]

Fig. 3 shows the block diagram of the series control where the series converter generates the real and reactive power at the transmission line using the dc-link capacitor voltage. This control strategy only takes two reference values of P_{ref} and Q_{ref} and also compares P_{ref} and Q_{ref} with $V_{d,\ grid}$ to derive $I_{d,ref}$ and $I_{q,\ ref}$ [7] as expressed by equations (1-2)

$$I_{d,\ ref} = \frac{\left(V_d{}^*P_{ref}\right) + \left(V_q{}^*Q_{ref}\right)}{\sqrt{(V_d)^2 + (V_q)^2}} \quad (1)$$

$$I_{q,\ ref} = \frac{\left(V_d{}^*P_{ref}\right) - \left(V_q{}^*Q_{ref}\right)}{\sqrt{(V_d)^2 + (V_q)^2}} \quad (2)$$

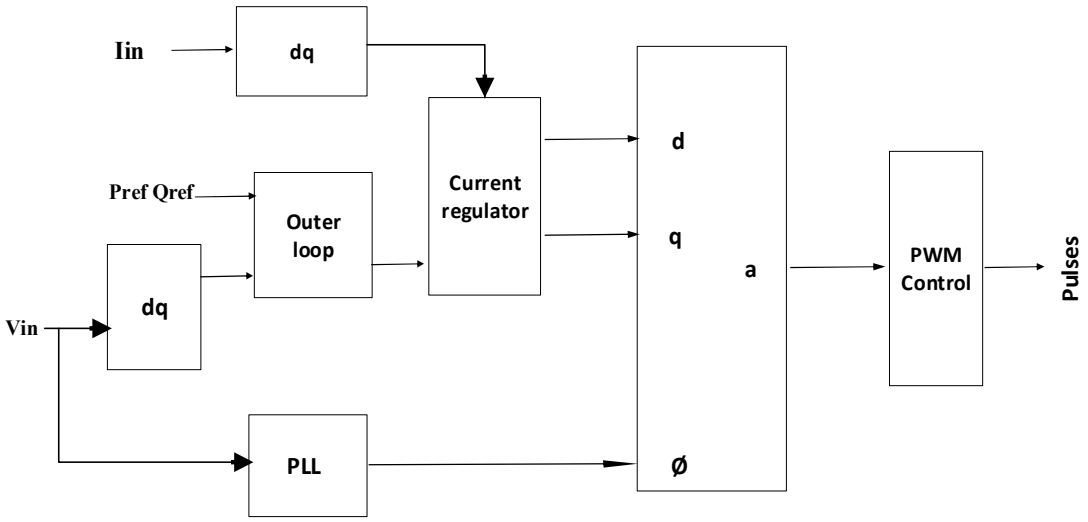

Fig. 3: UPFC series control block diagram [7]

2.2 DPFC Concepts

The Distributed Power Flow Controller (DPFC) is a new voltage and power stability enhancement concept developed from the UPFC [8-9]. The DPFC operates without a common dc-link between the UPFC shunt and series converters.

However, it utilizes the distributed FACTS concept related to the UPFC, which involves splitting the three-phase series converter into several single-phase series distributed converters via the transmission lines [10]. The DPFC compensates for real and reactive power flow using a shunt and many series-connected converters. In contrast, each converter operates autonomously, and their respective D.C. capacitors provide the needed D.C. voltage. The UPFC achieves its voltage stability enhancement and improvement of power (real and reactive power) transfer capability by the end-to-end connections of the shunt-series converters. In addition, the DPFC eliminates the D.C. link between the shunt-series converters to maintain the same control capability as the UPFC and presents the non-sinusoidal voltage and current as the expression of the sum of the sinusoidal components at different frequencies based on the Fourier analysis. The active power produced is due to the product of the voltage and current parameters. Because the integral of one or two terms with different frequencies is zero, resulting in the active power expression [9-10] as in equation 1.

$$P = \sum_{i=1}^{\infty} V_i I_i \cos cos \emptyset_i \quad (3)$$

Equation (1) shows the active power at different frequencies is autonomous of each other, such that V_i and I_i represent the voltage and current of the i^{th} harmonic frequency and $\emptyset_i$ is the angle between the voltage and current, leaving the converter with the possibility of absorbing the active power in one frequency and generating it in the other frequency. However, incorporating the DPFC into the transmission network can result in the shunt converter absorbing the active power at the fundamental frequency from the grid and injecting the current back into the grid at the harmonic frequency, thus, enhancing the flow of harmonic current via the transmission network.

Consequently, in a three-phase system, the third harmonic in each phase is equal and is referred to as the zero-sequence, where the shunt-series converters, high pass filter, and the ground form the closed loop for the harmonic current. In theory, the third, sixth, and ninth-harmonic frequencies enhance the active power exchange of the DPFC because they are all zero-sequence.

Grounding the star-delta transformer approach can be significant for routing the harmonic current in a meshed network.

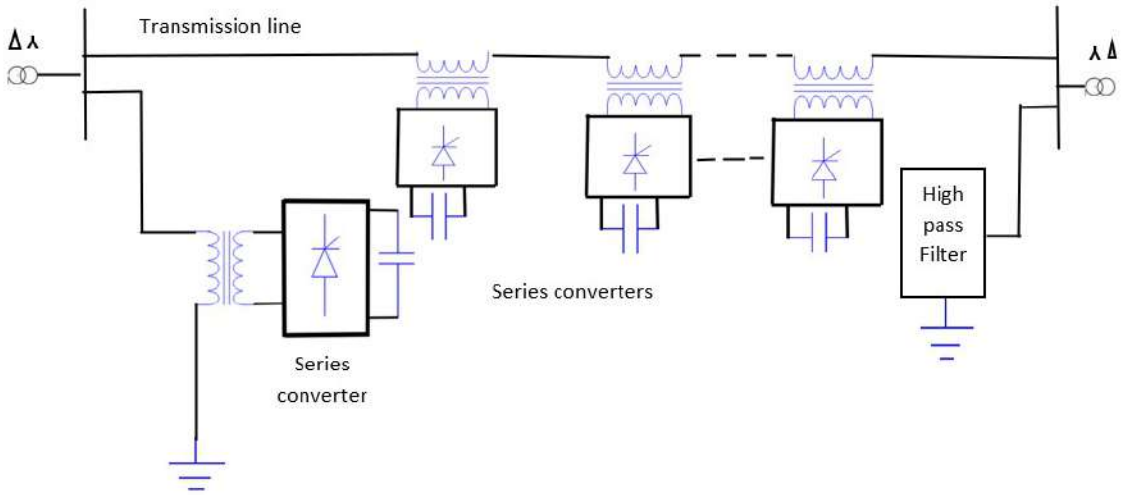

Fig. 2: Basic DPFC Circuit Arrangement

In Fig. 2, the small-sized single-phase converters rating makes the operation of the DPFC less expensive, coupled with higher reliability provided by the large numbers of series converters and improved system parameters controllability capacity compared to UPFC, which works with three-phase converters [11]. The DPFC comprises one shunt and numerous series-connected converters that can freely enhance the effective regulation capability and power flow control with lesser harmonics.

Fig. 3 shows the block diagram of the shunt control of the back-to-back configuration connection between the three-phase shunt converter and the two single-phase shunt converters. In this control system, the fundamental grid frequency absorbs the active power of the converter, and aside from this, it enhances the adjustment of the dc voltage between the capacitor and the single-phase converters and provides the shunt converter with a third harmonic current via the neutral wire of the Y transformer.

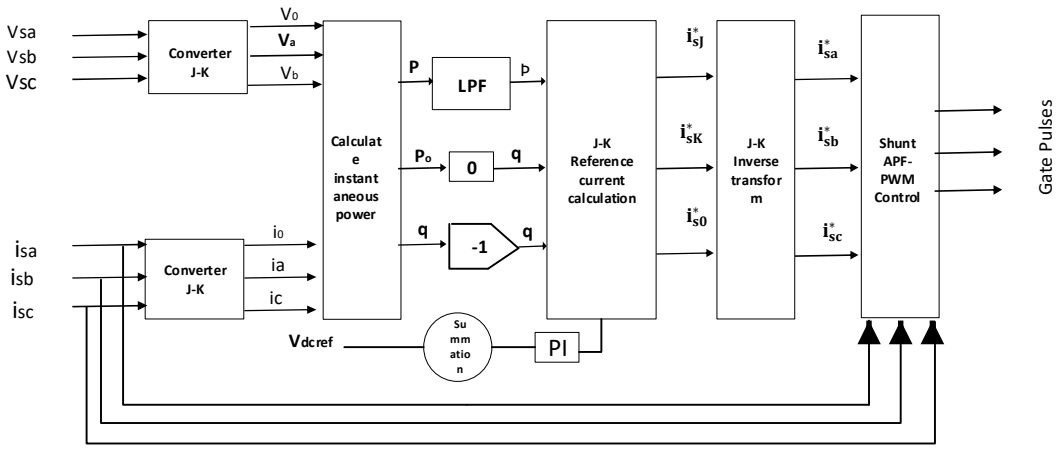

Fig. 3: DPFC shunt control block diagram [11]

Fig. 4 shows the block diagram of the series control where a separate series control achieves the control of each single-phase converter throughout the transmission line. In addition, during the d-q frame, the voltage of the sequence capacitor, the line current, and the series voltage reference serve as the controller input [12, 13, 14].

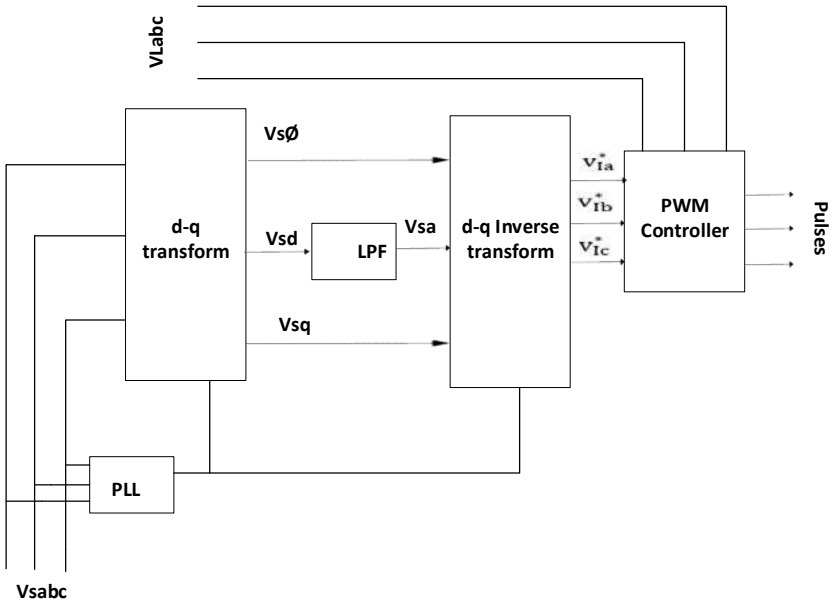

Fig. 4: DPFC Series Control Block Diagram [12, 13, 14]

III. COMPARISONS BETWEEN UPFC AND DPFC

The objectives of the FACT devices of UPFC and DPFC are equal, while their working principles differ. DPFC principle achieves the active power exchange between the shunt-series converters at the third harmonic frequency. Also, it enhances the respective series converters' active and reactive power compensation capability of the transmission line. In DPFC, a power line or transmission line can also transfer electrical power at the third harmonic frequency between DPFC transformers [15]. The UPFC has two three-phase converters linked back-to-back series using a common D.C link. UPFC principle achieves power flow reliability through the line by efficiently adjusting the transmission line's voltage magnitude, angle, and impedance. The performance improvement of the UPFC and DPFC in changing voltage stability and power flow regulation through the line reduces overall harmonic distortion by minimally updating the transmission network parameters.

Table 1: Operational Comparisons of UPFC and DPFC

Particulars	UPFC DEVICE	DPFC DEVICE
Control Capability	Low	High
Operational Reliability	Low	High
Noise Problem	Noisy	Less noisy
Electrical Efficiency	Less efficient	Very efficient
Converter	Two Three-phase	One single shunt and multiple independent series
Dc link	Present	None
Power Quality and Stability	Medium	High
Cost	Expensive due to three-phase converters ratings	Less expensive due to single-phase converters rating
Harmonic Problem	Reduced	Effectively reduced
Fault Response	High	Very high

The primary significance of the UPFC is controlling the active power and reactive power flow through the injection of the voltage in series with the transmission line and separately varying both the magnitude and the phase angle. Thus, the UPFC is helpful in the transient improvement and moderate power system signal stability [16].

IV. SIMULATION RESULTS

The simulation of UPFC and DPFC are performed using the MATLAB/SIMULINK software, the simulation results of UPFC and DPFC are investigated, analyzed, and compared in the work. Table 2 shows the parameters of the simulation.

Table 2: Simulation Parameters

Parameter	Value
V_s L-L	380 V
V_L L-L	380 V
Line Impedance (L)	5 mH
Load power	20 kW
Frequency	50 Hz
Cse	1.8 mF
Csh	1.8 mF
Vdc	658 V

Fig. 5 shows the simulated SIMULINK/MATLAB model of the DPFC with the shunt and series converters.

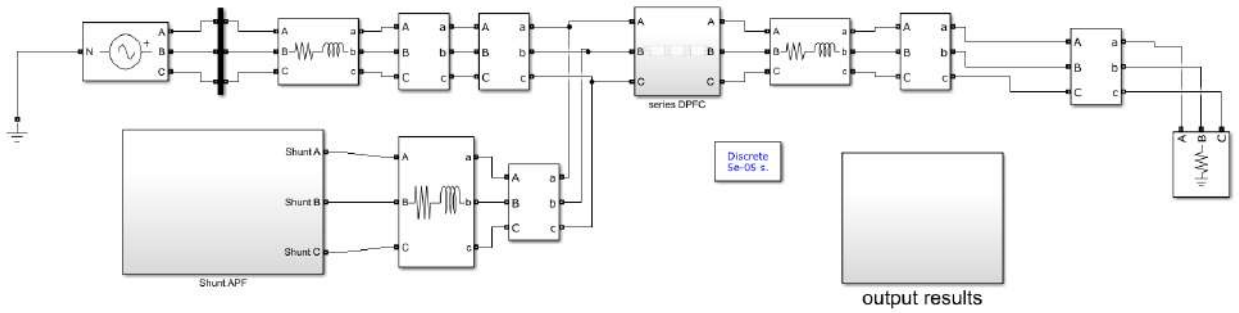

Fig. 5: Simulated Model of DPFC in MATLAB/SIMULINK

Fig. 6 shows the voltage sag and swell on grid voltage without a DPFC device. In addition, the effects of the phase shift on the load voltage are because of the voltage sag and voltage swell that negatively affect the various load-connected equipment, thus limiting the reliability and quality of electrical power transmission.

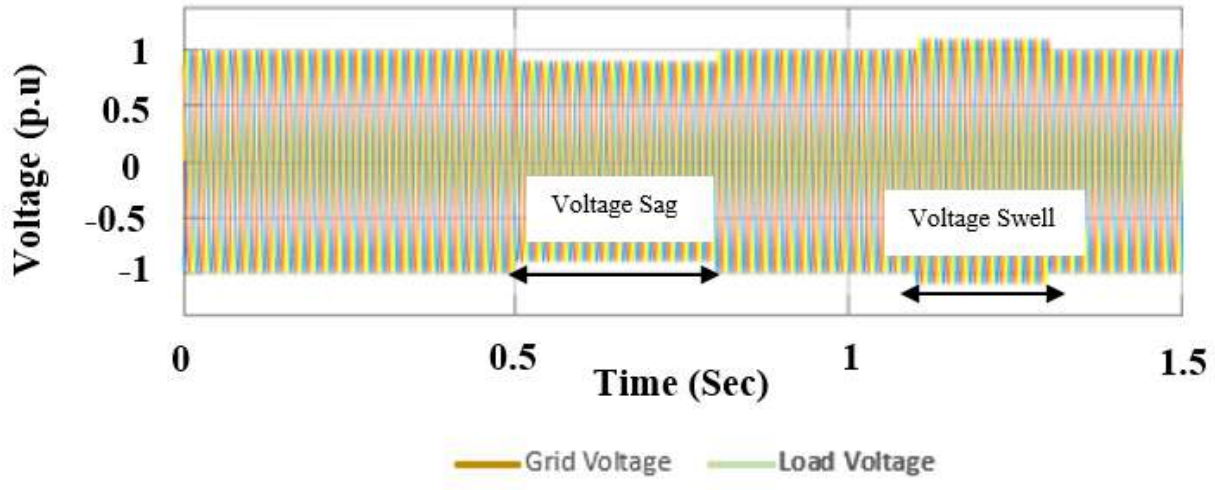

Fig. 6: Grid voltage waveform without DPFC device

Fig. 7 shows that voltage sag and swell effects are mitigated by incorporating the DPFC device that eliminates phase shift impact to enhance the power transfer capability of the transmission systems controllability and improve system power flow.

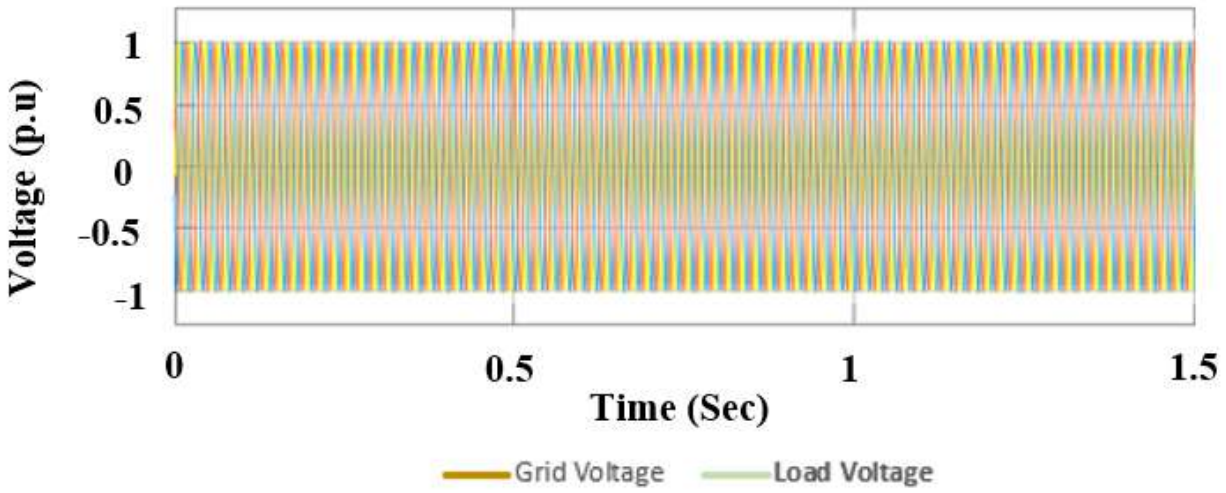

Fig. 7: Grid voltage waveform with DPFC device

The series converters improve the system voltage profile, while the shunt converters control reactive power flow to maintain a constant D.C. capacitor voltage throughout the operation.

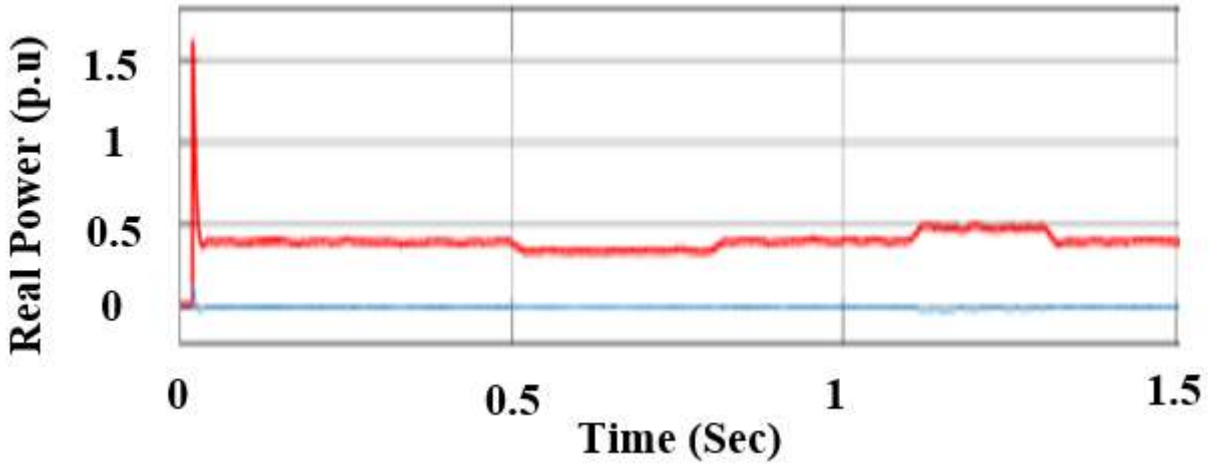

Fig. 8: Real source power response per unit of DPFC device

Fig. 8 shows the waveform of the real power response per unit of DPFC where the shunt's and series converters' injected power compensate for the increasing system voltage sag and voltage swell.

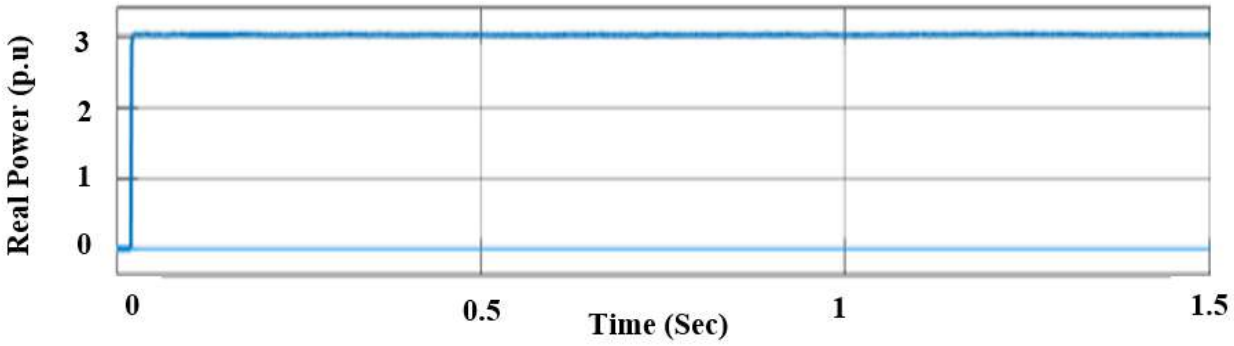

Fig. 9: Real load Power Response per unit of DPFC Device

Fig. 9 shows the waveform of the real load power response per unit of DPFC, where the constant real power output waveform is due to the shunt and series converters' voltage compensation.

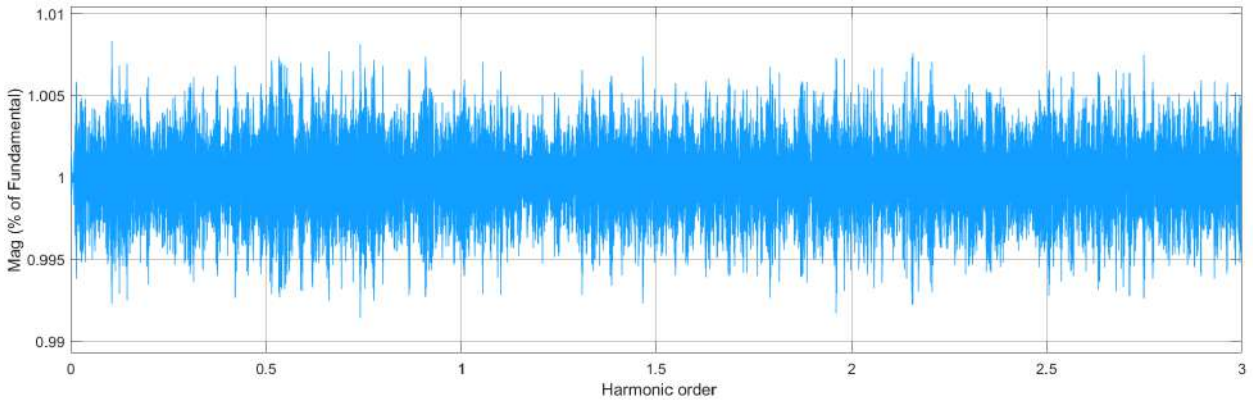

Fig. 10: DPFC device load current third harmonic distortion

In Fig. 10, it can be deduced that the third harmonic distortion drastically reduced to a lower value of up to 1.01%, which is considered acceptable since it's less than 5%, and this shows that the general power quality-related problems of voltage sag, voltage swell, and THD are mitigated.

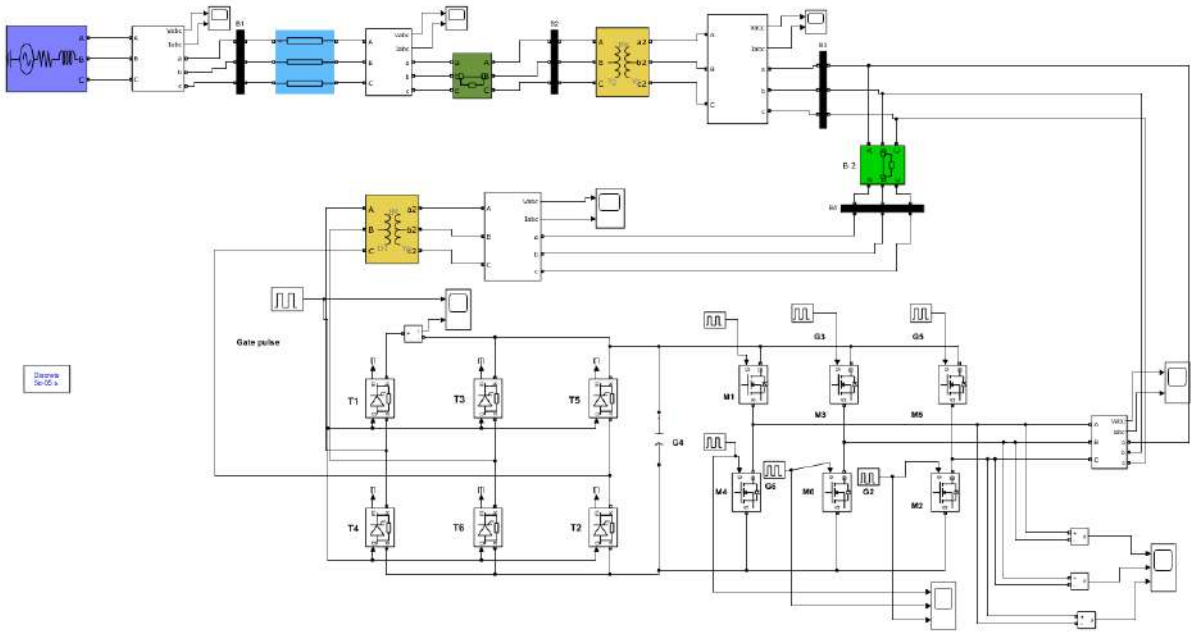

Fig. 11: Simulation result of voltage sag and voltage swell with UPFC device

Fig. 11 shows the SIMULINK/MATLAB simulation of the voltage sag and voltage swell based on the UPFC device.

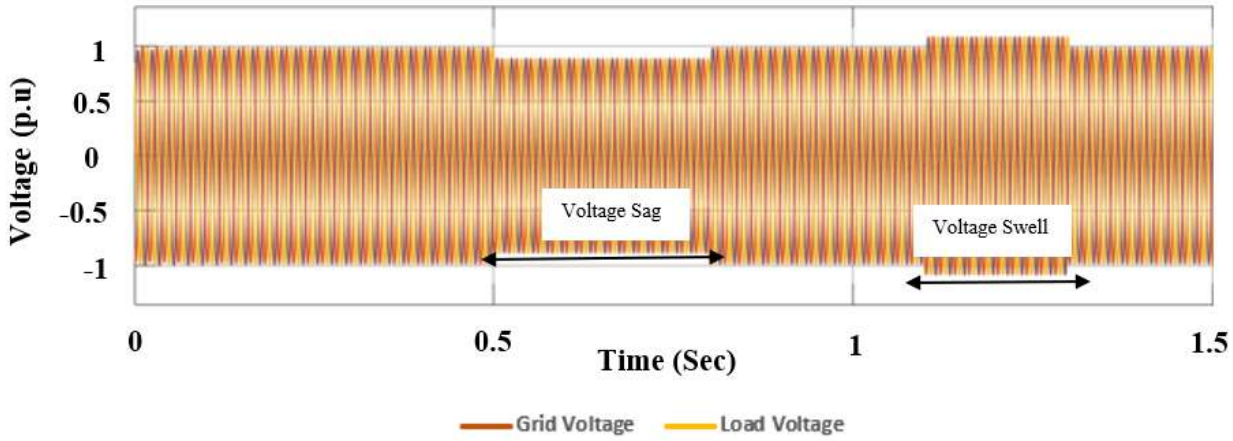

Fig. 12: Grid voltage waveform without UPFC device

In Fig. 12, the waveform of the voltage sag and voltage swell is because of the effects of the phase shift at the load voltage.

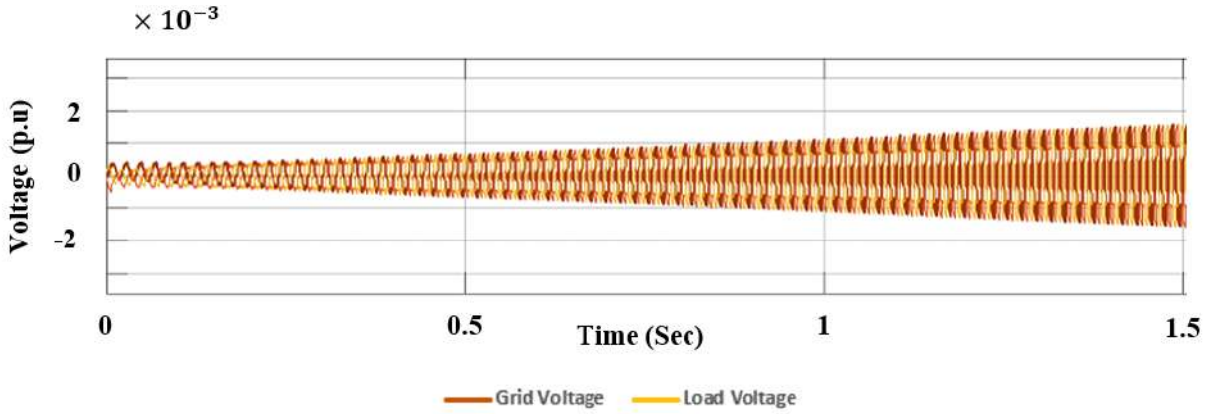

Fig. 13: Grid voltage waveform with UPFC device

In Fig. 13, the load voltage waveform shows no voltage sag and voltage swell due to the elimination of phase shift by installing a UPFC device that controls voltage magnitude and phase angle.

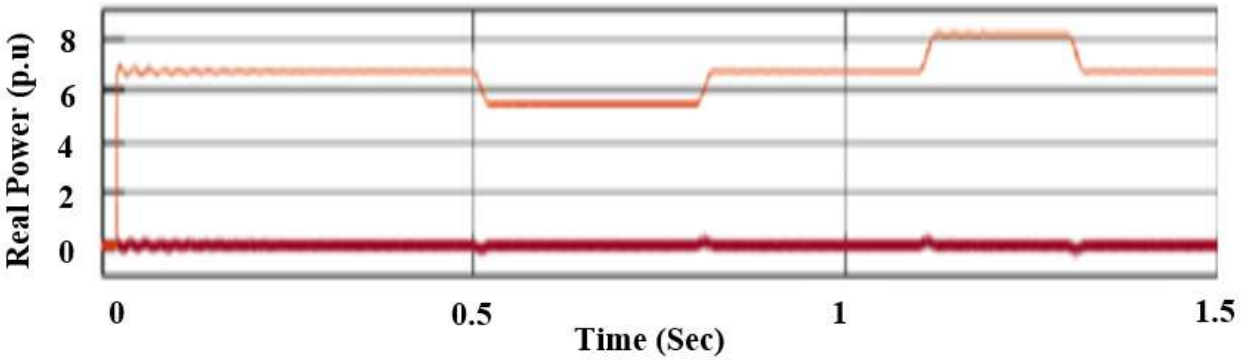

Fig. 14: Real Source Power Response Per unit of UPFC Device

Fig. 14 shows the real source power response in which the UPFC device provides control of real power flow to improve the power transfer capability of the system.

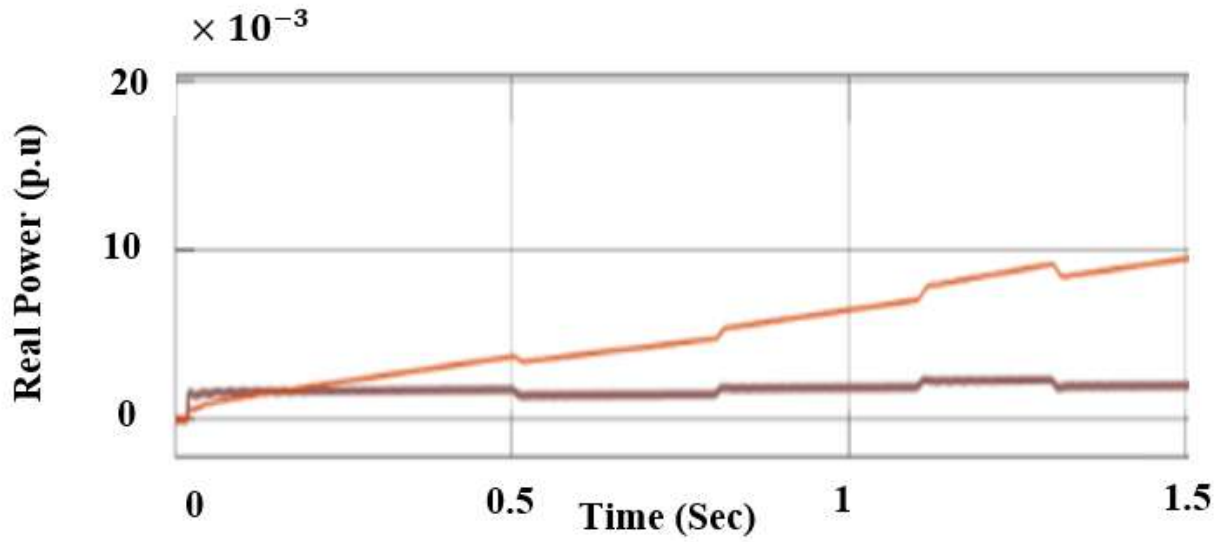

Fig. 15: Real Load Power Response per unit of UPFC Device

Fig. 15 illustrates the real load power response due to the addition of the UPFC device that provides power flow modulation in the system.

The simulation results show that the DPFC device performs better than the UPFC in control of the power flow profile.

V. CONCLUSIONS

The FACTS devices of UPFC and DPFC are the most versatile power factor compensators due to their excellent performance in mitigating power quality problems of voltage sag, voltage swell, voltage fluctuations, voltage imbalance, harmonics, and so on. The Matlab/Simulink simulation results show that the UPFC enhances the control of the real and reactive power flow with an injection of voltage in series with the transmission line due to the autonomous variation in both the magnitude and the voltage phase angle. Also, the UPFC can be used in the power system for transient stability of the small signal improvement. The Matlab/Simulink simulation results show that DPFC can perform better than UPFC because it provides additional flexibility by eliminating the dc-link between the shunt and the series converters. In addition, it has a low rating due to splitting the three-phase series converters into smaller single-phase converters distributed between the transmission line, which eliminates the requirement for high-voltage isolation, lower cost, and makes it simple to construct. The simulation results also demonstrate that the DPFC device can effectively reduce voltage sag and swell compared with the UPFC device. Moreover, the DPFC device can significantly reduce the third harmonic distortion in the power system.

REFERENCES

1. K. K. Sen, and M. L. Sen, "Introduction to FACTS Controllers: Theory, Modelling, and Applications, " Hoboken, NJ: John Wiley, 2009.
2. N. G. Hingorani and L. Gyugyi, "Understanding FACTS: Concepts and Technology of Flexible A.C. Transmission System, "Wiley-IEEE Press, 1999.
3. L. Gyugyi, C. D. Schauder, S. L. Williams, T. R. Rietman, D. R. Torgerson, and A. Edris, "The unified power flow controller: a new approach to power transmission control," IEEE Trans. Power Del., vol. 10, no. 2, pp. 1085–1097, Apr. 1995.
4. Samir Abood, "Fundamental of Electric Power System," A Primer with Matlab," Energy Science, Engineering and Technology, Nova Science and Technology, 2021.
5. L. Gyugyi, "Unified power-flow control concept for flexible A.C. transmission systems," Proc. Inst. Elect. Eng., Gen.,

Transm., Distrib., vol. 139, no. 4, pp. 323–331, Jul. 1992.
6. R. K. Verma and R. Salehi, "SSR Mitigation with a New Control of P.V. Solar Farm as STATCOM (PV-STATCOM)," IEEE Transaction on Sustainable Energy, Vol 8, Issue 4, pp.1473-1483, Oct. 2017.
7. A. Sen, A. Bernajee, H. Nannam, "A Comparative Analysis between UPFC and DPFC in a Grid-Connected Photovoltaic System," IEEE International Conference on Intelligent Techniques in Control, Optimization and Signal Processing (INCOS), vol. 10, no. 9, pp. 1- 6, Apr. 2019.
8. K. H. Song and A. Johns, "Flexible ac Transmission Systems (FACTS) (IEEE Power and Energy Series), vol. 30. London, U. K: Institution of Electrical Engineers, 1999.
9. Z. Yuan, S. W. H de Haan, B. Ferreira, and D. Cevoric, "A FACTS Device: Distributed Power Flow Controller (DPFC), "IEEE Transaction on Power Electron., vol.25, no.10, Oct. 2010.
10. A. Jamshidi, S. M. Barakati, and M. M. Ghahderijani, "Impact of Distributed Power Flow Controller to Improve Power Quality Based on Synchronous Reference Frame Method," LACSIT International Journal of Engineering and Technology, vol. 4, no. 5, Oct. 2012.
11. M. A. Hannan, "PSCAD/EMTDC Simulation of Unified Series-Shunt Compensator for Power Quality Improvement", IEEE Transactions on Power Delivery, vol. 20, no. 2, Apr. 2005.
12. D. Celik, and M. E. J. C. E. P. Meral," Current control-based power management strategy for distributed power generation system," vol. 82, no. 10, pp. 72-85, Jan. 2019.
13. T. Kang, et al., "Series voltage regulator for a distribution transformer to compensate voltage sag/swell," vol. 64, no. 6, pp. 4501-4510, Feb. 2017.
14. B.V. Kumar, and V. J. E. Ramaiah," Enhancement of dynamic stability by optimal location and capacity of UPFC: A hybrid approach," vol.190, no. 4, pp. 116-464, Jan. 2020.
15. R. K Verma, R. Salehi, "SSR Mitigation with a New Control of P.V. Solar Farm as STATCOM (PV-STATCOM), " IEEE Transaction on Sustainable Energy, Vol 8, Issue 4, pp.1473-1483, Oct. 2017.
16. A. Sen, A. Bernajee, H. Nannam," A Comparative Analysis between UPFC and DPFC in a Grid-Connected Photovoltaic System," IEEE International Conference on Intelligent Techniques in Control, Optimization and Signal Processing (INCOS), vol. 10, no. 9, pp. 1-6, April 2019.

Relationship between Asphalt Concrete Linear Stress Limit and Bitumen Shear Stress Limit

Victor Zolotaryov

Automobile and Highway University

ABSTRACT

The rheological behaviour of asphalt concrete is mostly stipulated by the time-temperature (frequency) peculiarities of the mechanical behaviour of bitumen binder. Bitumen is among the first item of research in rheological science.

One criteria of the objective evaluation of the rheological properties of bitumen is realised in the condition of its deformation in the linearity region.

In relation to asphalt concrete, this criterion allows the applicability of the method of time-temperature superposition according Williams- Landel-Ferry model for complex moduli and their dependence on the composition of asphalt concrete and type of bitumen (sol, gel, or sol-gel) to be proven. Also, it can show the direct relation between complex moduli of asphalt concrete and the complex shear modulus of bitumen binder, providing a method of calculation of the complex modulus of asphalt concrete with the complex shear modulus of bitumen. However, it is not clear on which parameters of bitumen and bituminous binder properties the asphalt concrete linear viscoelastic LVE behaviour depends directly.

Keywords: bitumen binder, asphalt concrete, penetration, linear viscoelastic behaviour, LVE stress limit, shear strength.

Classification: DDC Code: 665.4 LCC Code: TP690

Language: English

London Journals Press

LJP Copyright ID: 392953
Print ISSN: 2631-8474
Online ISSN: 2631-8482

London Journal of Engineering Research

Volume 22 | Issue 9 | Compilation 1.0

Relationship between Asphalt Concrete Linear Stress Limit and Bitumen Shear Stress Limit

Victor Zolotaryov

ABSTRACT

The rheological behaviour of asphalt concrete is mostly stipulated by the time-temperature (frequency) peculiarities of the mechanical behaviour of bitumen binder. Bitumen is among the first item of research in rheological science.

One criteria of the objective evaluation of the rheological properties of bitumen is realised in the condition of its deformation in the linearity region.

In relation to asphalt concrete, this criterion allows the applicability of the method of time-temperature superposition according Williams-Landel-Ferry model for complex moduli and their dependence on the composition of asphalt concrete and type of bitumen (sol, gel, or sol-gel) to be proven. Also, it can show the direct relation between complex moduli of asphalt concrete and the complex shear modulus of bitumen binder, providing a method of calculation of the complex modulus of asphalt concrete with the complex shear modulus of bitumen. However, it is not clear on which parameters of bitumen and bituminous binder properties the asphalt concrete linear viscoelastic LVE behaviour depends directly.

This paper aims to illustrate that this parameter is the maximal shear stress in bitumen binder, which is obtained with the same asphalt concrete temperatures and frequencies or equal deformation rates. Considering this, maximal shear stress can be obtained with monoplanar or rotational shear, as with the calculation method.

This research uses a monoplanar cohesion meter, a rotational viscometer, and test equipment to determine the complex moduli of asphalt concrete by means of harmonic oscillation, corresponding to EN 12697-26:2012.

Keywords: bitumen binder, asphalt concrete, penetration, linear viscoelastic behaviour, LVE stress limit, shear strength.

Author: Doctor of Technical Sciences, professor of Kharkiv National Automobile and Highway University. 61002, Ukraine, Kharkov, st. Yaroslava Mudrogo, 25 kafedradsm@gmail.com

I. СОСТОЯНИЕ ВОПРОСА И ЦЕЛЬ ИССЛЕДОВАНИЯ

Основным условием обеспечения надежности работы дорожных слоев является их способность к обратимому восстановлению деформаций, вызванных транспортными нагружениями. Эта способность сохраняется в тех случаях, когда связь между возникающими в слое напряжениями и деформациями при определенных скоростях или частотах деформирования является линейной, т.е. когда материалы слоев не выходят за пределы области линейного вязкоупругого (ЛВУ) поведения. Для объективного прогнозирования реологического поведения асфальтобетона целесообразно использовать характеристики его линейного состояния, которые можно установить по границам линейной зависимости между напряжением и деформацией.

Обнаружение области линейного поведения асфальтобетона открыло возможность изучения взаимосвязи между комплексными модулями асфальтобетонов и комплексными модулями сдвига битумных вяжущих.

Экспериментальные степенные зависимости между комплексными модулями и частотой деформирования были получены в работах [1, 2, 3, 4]. Позже были предложены модели расчета температурно- частотных зависимостей комплексных модулей

асфальтобетона по соответствующим показателям, вяжущих [5].

Несмотря на огромный поток информации по рассматриваемому научному направлению, одна из его сторон до сих пор осталась неизученной, а именно, взаимосвязь критического напряжения ($\sigma_{ЛВУ}$) или критической деформации ($\varepsilon_{ЛВУ}$) линейности асфальтобетона с реологическими или техническими показателями битумов.

Существуют работы, в которых приводятся зависимости модулей упругости от пенетрации [6, 7] но это не решает проблему.

После публикации исследований [8, 9] предварительное определение области линейной вязкоупругости стало обязательным при изучении температурно-частотных зависимостей любых асфальтобетонов.

Границей линейности в [2] было принято отклонение комплексного модуля асфальтобетона от начального его значения на 5 %. Это же требование принято и в [3, 4].

Развиваемые в этом направлении исследования раскрыли одну из особенностей изменения критериев линейности асфальтобетона с частотой и температурой.

Она состоит в том, что предельные напряжении линейности ($\sigma_{ЛВУ}$) более чувствительны к частоте деформирования, чем предельные деформации ($\varepsilon_{ЛВУ}$). Согласно данным [3, 4] с ростом частоты деформирования от 0,01 Гц до 20 Гц при температуре 20 °С $\varepsilon_{ЛВУ}$ возрастает в 1,2 раза, $\sigma_{ЛВУ}$ – 8-10 раз. Согласно [1] при изменении частоты на 2 порядка (от 0,1 Гц до 10 Гц) и той же температуре $\varepsilon_{ЛВУ}$ возрастает в 1,29 раза, а критическое напряжение ($\sigma_{ЛВУ}$) – в 7,8 раз.

Значение этих характеристик изменяется с температурой. При прочих равных условиях, по данным [3, 4] повышение температуры от 10 °С до 40 °С понижает σ_{LVE} почти в 16 раз, в то время как $\varepsilon_{ЛВУ}$ мало зависит от температуры и частоты деформирования [10].

Это подтверждается также данными [11] из которых следует, что с ростом комплексного модуля $E^*_{ЛВУ}$ критическое напряжение асфальтобетона растет в 2,6 раза больше, чем критическая деформация. Согласно [12] это соотношение равно 2,4, а согласно [13] – 1,8 раза.

С учетом накопившихся к настоящему времени сведений об обусловленности реологического поведения асфальтобетона реологическими свойствами битума целью настоящей работы является установление взаимосвязи между предельными напряжениями асфальтобетона (σ_{LVE}) и предельными напряжениями сдвига битума ($\tau_б$).

II. ОБЪЕКТЫ ИССЛЕДОВАНИЙ

В качестве вяжущих для исследований использованы: битумы различной консистенции; битумы, полученные окислением и вакуумной дистилляцией; битумы, модифицированные полимерами (табл. 1).

Таблица 1: Свойства принятых к исследованию вяжущих

Битумы	Полимер	%	Свойства вяжущих					Обозначения
			$П_{25}$, дм	$Т_р$, °С	IP	$Т_{хр}$, °С	$Е_{25}$, %	
1	SBS линейный	0	46	56	0,0	-15	–	○
		3	30	72	1,92	-15	77	●
2	SBS линейный	0	70	51	-0,11	-18	–	△
		3	46	66	1,94	-18	80	▲
3	SBS линейный	0	116	46	0,01	-20	–	◇
		3	60	55	0,44	-20	86	◆
		5	48	80	4,21	-19	95	■

		7	40	91	5,11	-28	95	▲
	SBS радиальный	3	70	59	1,74	-19	88	●
	EVA	5	76	53	0,62	-20	57	+
4	SBS линейный	0	176	39	-1,04	-23	–	□
		3	66	52	-0,02	-21	90	■
		3	126	47	0,64	-25	93	
5		0	57	54	-0,20	-16	–	
		0	72	50	-0,7	-17	–	
		0	120	45	-0,5	-18	–	
		0	170	42	-0,4	-19	–	

Минеральный порошок, полученный помолом известняка, содержал зерен мельче 0,071 мм – 72 %. Гранулометрический состав минеральной части исследованного асфальтобетона типа Б характеризовался: полными остатками на ситах с размером круглых отверстий (мм): 10, 5; 2,5, 1,25, 0,63, 0,315, 0,14, 0,071 соответственно (20, 40, 53, 63, 72, 80, 86 и 89) %. Содержание вяжущего в такой смеси было в пределах 4,8-5,0 %, сверх 100 % минеральной части. Критерием назначения содержания вяжущего было то его количество, при котором прочность асфальтобетона на сжатие при 20 °С была максимальной.

III. МЕТОДЫ ИССЛЕДОВАНИЙ

Битумные вяжущие:
Среди предполагаемых показателей свойств вяжущих, которые могут быть взаимосвязаны с характеристикой $\sigma_{ЛВЕ}$ асфальтобетона, как показано выше, предпочтительным является сопротивление сдвигу и когезия.

Сопротивление сдвигу определяли при деформировании вяжущего в зазоре ротационного вискозиметра при скорости равной $1с^{-1}$ и температуре 25 °С по методу EN 13302:2010.

Когезию при сдвиге определяли методом одноплоскостного сдвига пленки вяжущего в слое толщиной 200 мкм при тех же температуре и скорости сдвига.

Сопротивления сдвига, установленное таким образом, согласуется с сопротивлением сдвига, установленным методом ротационной вискозиметрии [14].

Асфальтобетоны: Реологические свойства асфальтобетонов исследовали методом гармонических колебаний в соответствии с EN 12697-26 [15] по схеме изгиба двумя сосредоточенными силами[8, 9]. При такой схеме напряженного состояния имеется возможность измерять очень малые относительные деформации, начиная от $1x10^{-5}$. Испытания выполняли в диапазоне температур – от минус 25 °С до плюс 30 °С и частот от 0,01 Гц до 20 Гц.

Каждому испытанию по определению комплексных модулей в широком диапазоне частот и температур предшествовало определение зависимости между усилиями и прогибами. Предельным напряжением линейности считали участок, в пределах которого отклонение от линейности не превышало 10 %. Типичные диаграммы напряжение – деформация и схема определения $\sigma_{ЛВУ}$ $\varepsilon_{ЛВУ}$ при температуре 20 °С и частоте 0,5 Гц приведены на рис.1.

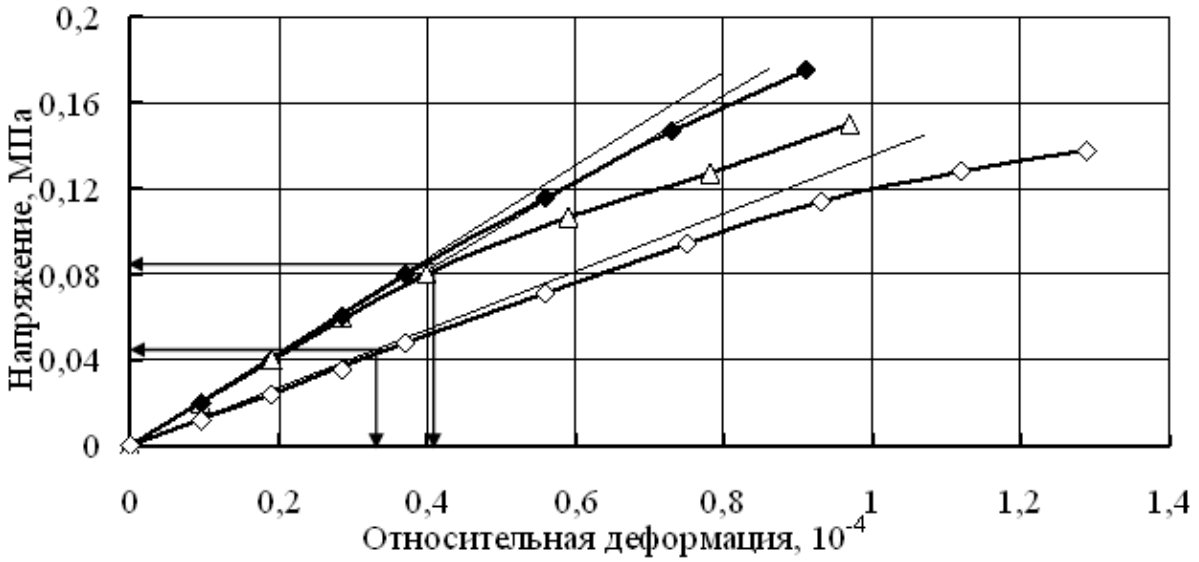

Рис. 1: Зависимость между напряжениями ($\sigma_{ЛВУ}$) и деформациями ($\varepsilon_{ЛВУ}$) асфальтобетона на вяжущих с разной пенетрацией: ◇ - 116 × 0,1 мм; △ - 70 × 0,1 мм и БМП ⋄ - 60 × 0,1 мм

3.1 Экспериментальная зависимость предельных напряжений линейности ($\sigma_{ЛВУ}$) асфальтобетона от пенетрации битума

Исторически при исследовании асфальтобетона на протяжении 50 лет в первую очередь уделяли внимание зависимости его механических свойств от пенетрации битумов. Для принятых объектов исследования зависимости $\sigma_{ЛВУ}$ от пенетрации [16] показаны на рис.2. Рост пенетрации вяжущего приводит к существенному снижению $\sigma_{ЛВУ}$ асфальтобетона на его основе.

С повышением пенетрации от 46 до 70 dmm, 116 dmm и 176 dmm (т.е. в 1,52; 2,56 и 3,82 раза) критическое напряжение $\sigma_{ЛВУ}$ уменьшается в 1,73, 3,22 и 5,9 раза. При этом критическая деформация линейности $\varepsilon_{ЛВУ}$ уменьшается в 1,42; 1,76 и 2,62 раза. При близкой пенетрации вяжущие (чистый битум – 46 dmm; битум с $П_{25}$=70 dmm и с 3 % полимера – $П_{25}$=46 dmm; битум с пенетрацией 116 dmm и с 5 % полимера –$П_{25}$=48 dmm) имеют критические напряжения (σ_{LVE}) асфальтобетонов линейности соответствовали 0,142 МПа, 0,140 МПа и 0,144 МПа.

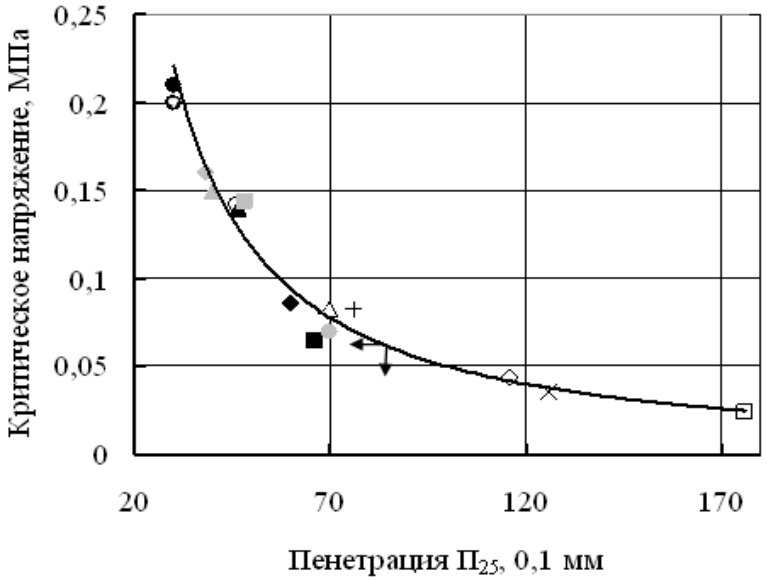

Рис. 2: Взаимосвязь между критическим напряжением линейности σ_{LVE} асфальтобетонов и асфальтополимербетонов (при температуре 20 °С и частоте 0,5 Гц) и пенетрацией вяжущих (условные обозначения приведены в табл.1)

Для зависимости, приведенной на рис.2, переход от резко ниспадающей ветви к плавно изменяющейся части зависимости обусловлен конусностью пенетрационной иглы и отвечает пенетрации (60-70) dmm.

Эта зависимость свидетельствует о безусловной связи пенетрации с σ_{LVE} асфальтобетона. Она подобна множеству зависимостей от пенетрации прочности, модулей жесткости, колеестойкости асфальтобетона. Однако все они остаются условными настолько, насколько пенетрация является условной эмпирической характеристикой. Именно поэтому пенетрация исключена из системы SHRP Superpave и в нее введена фундаментальная характеристика модуля сдвига битума.

Учитывая это, целесообразно установить объективную, метрологически обоснованную связь между $\sigma_{ЛВУ}$ асфальтобетона и характеристикой, отражающей сопротивление сдвига битума при заданных температуре и скорости деформирования. Его можно определить экспериментально, как описано выше или расчетом по методике, приведенной в [17].

3.2 Степенные зависимости $\sigma_{ЛВУ}$ от частоты деформирования

Предельным напряжениям линейной вязкоупругости асфальтобетонов присуща принципиальная особенность, характерная для всех вязкоупругих систем и выражающаяся в зависимости их реологических характеристик от скорости, частоты или времени деформирования. Как правило, эти зависимости являются степенными (рис.3). Для асфальтобетонов на битумах разной консистенции, полученных из одной нефти способом окисления, коэффициенты частотной зависимости практически одинаковы. Приведенная на рис.

3 прямая, обозначенная Δ, относится к асфальтобетону на использованном в работе [3] дистилляционном битуме с пенетрацией 49 х0,1 мм и температурой размягчения – 52 °С.

Это может объясняться тем, что у него наиболее низкий индекс пенетрации (-0,76) по сравнению с другими, т.е он наиболее чувствителен к частоте деформирования и температуре. Он находится в области самых больших значений σ_{LVE}, т.к. использованный для получения асфальтобетона битум имел самую низкую, по сравнению с другими битумами, пенетрацию.

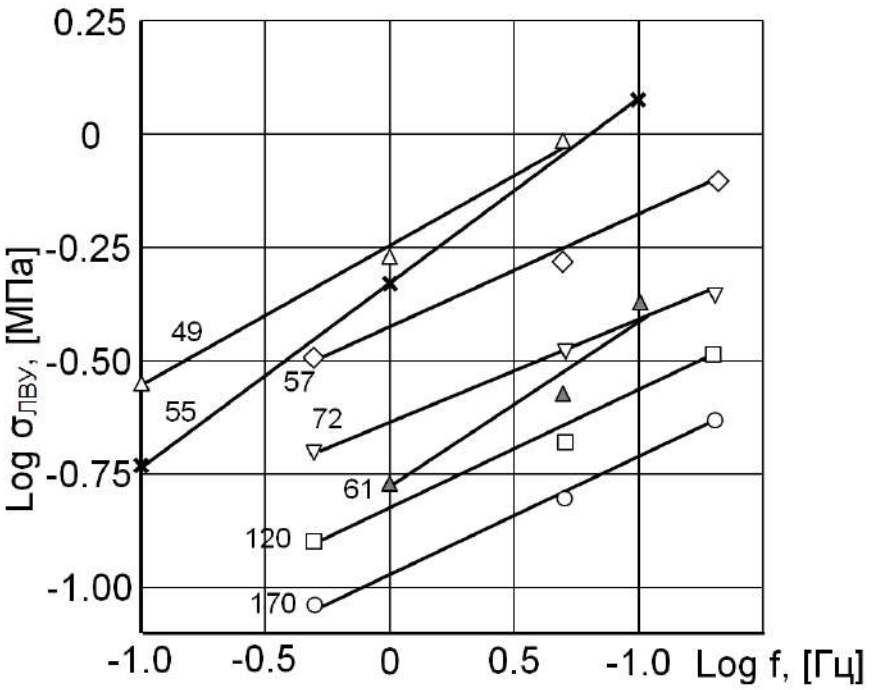

Рис. 3: Зависимость напряжения линейности (σ_{LVE}) от частоты (f) деформирования асфальтобетонов на битумах с разной пенетрацией при 20 °С (Цифры над прямыми – пенетрация при 25 °С)

Прямая, обозначенная ▲, получена обработкой данных [3]. Она относится к битуму, модифицированному радиальным SBS. Она расположена существенно ниже прямой, обозначенной Δ, поскольку в этом случае пенетрация БМП (61х0,1 мм) существенно больше пенетрации чистого битума ($П_{25}$=49х0,1 мм). При этом высокая температура размягчения БМП (72 °С) не повлияла на значение $\sigma_{ЛВУ}$, асфальтобетона.

Определяющим фактором влияния на $\sigma_{ЛВУ}$ является пенетрация. Прямая, обозначенная ×, получена обработкой данных [13]. Она достаточно хорошо согласуется с зависимостями для других вяжущих. Ее больший наклон, как и прямой обозначенной ▲, обусловлен тем, что вяжущие этих асфальтобетонов, как и все дистилляционные битумы, характеризуются большей температурной чувствительностью, чем окисленные битумы. Эти зависимости хорошо согласуются с полученными в [18] зависимостями модуля упругости асфальтобетона от времени действия нагрузки.

3.3 Взаимосвязь $\sigma_{ЛВУ}$ асфальтобетонов и предельного напряжения сдвига вяжущих.

Изначально, когда взаимосвязь $\sigma_{ЛВУ}$ асфальтобетона и предельного напряжения сдвига битумов еще не предполагалась, предельные напряжения асфальтобетонов были определены при температуре 20 °С, и частоте 0,5 Гц. Сопротивление сдвигу вяжущих при выполнении работ, имеющих целью установление взаимосвязи между когезией и пенетрацией, определяли, как отмечено выше, при температуре 25 °С и скорости сдвига 1 $с^{-1}$. Для целей же настоящей работы (обеспечения сопоставимости результатов обоих испытаний), возникла необходимость приведения $\sigma_{ЛВУ}$ асфальтобетонов к круговой скорости 1 $с^{-1}$ по формуле $\omega=2\pi f$. Приведение $\sigma_{ЛВУ}$ к температуре 25 °С было осуществлено по ранее установленному коэффициенту температурной чувствительности $\Delta \lg E^* / \Delta T$ между 20 и 30 °С [1]. Примеры такого приведения даны в табл. 2.

Таблица 2: Критические напряжения линейности $\sigma_{ЛВУ}$, приведенные к условиям, отвечающим условиям определения сопротивления сдвигу вяжущих

Битумные вяжущие, пенетрация при 25 °С	$\sigma_{ЛВУ}$ при 0,5 Гц и 20 °С, МПа	Показатель степенной зависимости $\sigma_{ЛВУ}$	$\sigma_{ЛВУ}$ при 20 °С и $\omega=1с^{-1}$, МПа	$\sigma_{ЛВУ}$ при 25 °С и $\omega=1с^{-1}$, МПа
Битум 70	0,082	0,20	0,065	0,061
БМП 46 (3 % СБС)	0,140	0,17	0,115	0,110
Битум 116	0,044	0,22	0,035	0,032
БМП 60 (3 % СБС)	0,086	0,18	0,070	0,066
Битум 176	0,024	0,24	0,018	0,016
БМП 66 (3 % СБС)	0,064	0,21	0,051	0,048

Взаимосвязь $\sigma_{ЛВУ}$ асфальтобетонов и предельного напряжения сдвига вяжущих (τ) приведена на рис. 4. Она может быть описана корреляционной зависимостью $\sigma_{LVE}=0,967\cdot\tau+0,0002$. Наличие такой зависимости с коэффициентом корреляции $R^2=0,951$ свидетельствует о непосредственном влиянии предельного напряжения сдвига, вяжущего на значение критических напряжений линейности асфальтобетона. При этом зависимость распространяется не только на чистые битумы, но и на битумы, модифицированные умеренным количеством полимера типа СБС. Следовательно, можно предполагать подобие механизмов деформирования пленок битума в когезионном слое и межзерновом слое в асфальтобетоне.

Результаты, относящиеся к асфальтобетонам на битумах, модифицированных полимерами, несколько выпадают из общей зависимости.

Такое отклонение может быть связано с изменением структуры и реологических характеристик вяжущих в результате модификации полимером [10]. На сложность использования подходов, принятых для битумов, к битумам с большим содержанием полимера обращали внимание в [19].

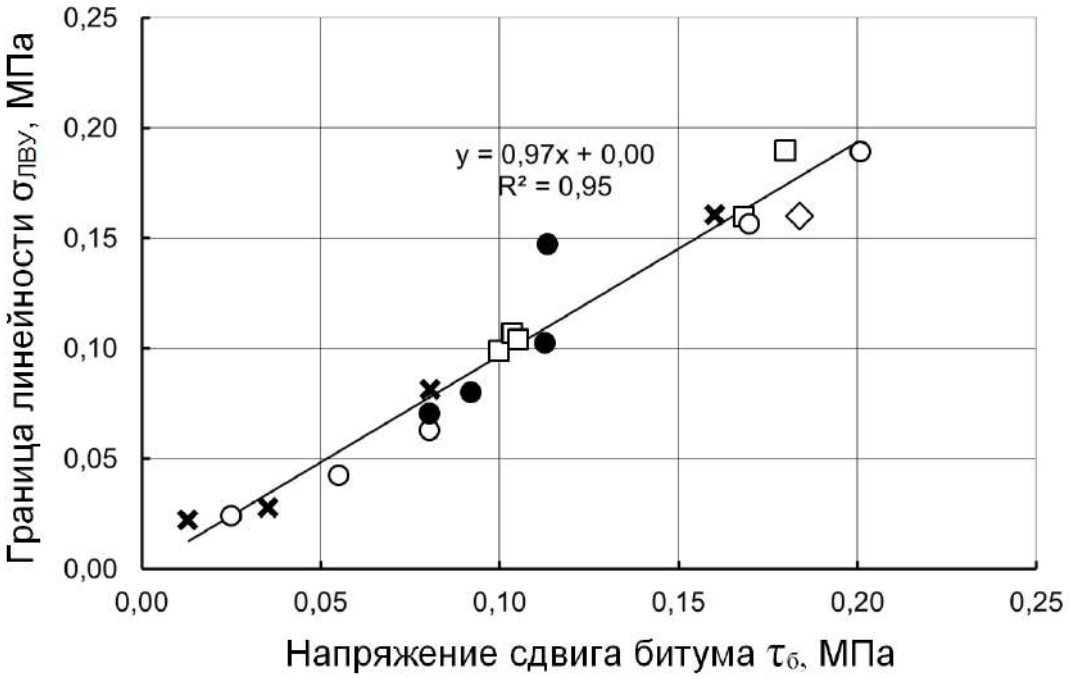

Рис. 4: Взаимосвязь между границей линейности (σ_{LVE}) асфальтобетонов и предельным сопротивлением сдвигу вяжущих при температуре 25 °C. Битумы с пенетрацией (0,1 мм): 57, 72, 120, 157 (×); битумы с пенетрацией (0,1 мм): 46, 70, 116, 176 (o); они же модифицированные 3 % полимера SBS (·); дистилляционный битум с пенетрацией 49 (0,1 мм) (◇) и модифицированный битум с пенетрацией 61 (0,1 мм) (◆) [2]; битумы, окисленные с пенетрацией: 50, 75, 105, 172 (0,1 мм), битумы дистилляционные Nynas с пенетрацией 52, 79, 118, 182 (0,1 мм) для которых когезия определена по пенетрационной зависимости (□) [17].

Дополнительным обстоятельством в пользу полученной зависимости является идентичность сопротивления сдвигу битума, определяемого при ротационных испытаниях [20], и модуля его потерь при эквивалентности круговой частоты и скорости сдвига, а также соответствие сопротивления сдвигу при ротационных измерениях и при одноплоскостном сдвиге [14]. Тем не менее, представляется предпочтительным, учитывая простоту эксперимента, прогнозировать $\sigma_{ЛВУ}$ асфальтобетона путём определения предельного сопротивления сдвига по результатам ротационной вискозиметрии и/или по когезии битумов, установленной при одноплоскостном сдвиге.

Приведенные здесь экспериментальные результаты свидетельствуют о необходимости углубленных исследований физической сущности деформирования битумов и асфальтобетонов на микроуровне в области малых деформаций и напряжений. Это находится в согласии с результатами работ [21, 22, 23, 24].

Требует обоснования практическое совпадение значений модулей упругости асфальтобетонов определяемых: при прямом растяжении и сжатии [25] при изгибе и сжатии [26]. Это относится и к податливости полых образцов при сжатии и непрямом (IDT) растяжении [27]. Обнадеживающим является утверждение, что значения комплексных модулей упругости в области малых деформаций (10^{-5}) не зависят ни от геометрии, ни от конфигурации испытаний [28]. Оно может восприниматься как одно из свидетельств справедливости изложенных здесь результатов исследований.

IV. ВЫВОДЫ

1. Способность асфальтовых бетонов к поведению, характерному линейным вязкоупругим телам, является базовым принципом конструирования и расчета

нежестких дорожных одежд. В соответствии с этим система оценки поведения асфальтобетона по реологическим критериям может быть дополнена характеристиками их линейного поведения: предельными напряжениями и деформациями.

2. Предельные напряжения линейного вязкоупругого поведения асфальтобетонов существенно более чувствительны к изменению свойств битумного вяжущего и внешним температурно-временным (частотным) воздействиям, чем предельные деформации линейности. Это позволяет более наглядно, чем в случае с $\varepsilon_{ЛВУ}$ отражать влияние на реологическое поведение асфальтобетона факторов состава и технологий.
3. Предельные напряжения линейности асфальтобетона, в изученном здесь диапазоне, находятся в степенной зависимости от частоты деформирования, подобно тому, как в этой же зависимости находятся их модули упругости, а также показатели прочности.
4. Установлена близкая к прямолинейной корреляционная зависимость между предельным сопротивлением битумного вяжущего сдвигу и предельным напряжениям линейного деформирования асфальтобетона. Она может быть использована для прогнозирования поведения асфальтобетона под нагрузкой в покрытии при заданной температуре и скорости деформирования.

ЛИТЕРАТУРА

1. Золотарев, В.А. Долговечность дорожных асфальтобетонов Харьков. 1977 116 с.
2. Anderson, D.A., Christenson, D.W., Bahia, H.V., Dongre, R., Sharma, M.G., Antle, C.E., & Button, J. (1994). Binder characterization and evaluation, vol. 3. Physical characterization. Report SHRP-A-369 (491 p.), Washington D.C.
3. Airey, G.D., Rahimzadeh, B., & Collop, A.C. (2002). Linear and nonlinear rheological properties of asphalt mixtures. Proceedings of the 4th European Symposium on the Performance of Bituminous and Hydraulic Materials in Pavements, Nottingham (pp. 137–145).
4. Airey, G.D., Rahimzadeh, B., & Collop, A.C. (2003). Viscoelastic linearity limits for materials. Proceedings of the 6th International RILEM Symposium. Performance Testing and Evaluation of Bituminous Materials (pp. 331–339).
5. Olard, F., Di Benedetto, H., Eckmann, B., & Triquigneaux, J.-P. (2003). Linear viscoelastic properties of bituminous binders and mixtures at low and intermediate temperatures. International Journal of Road Materials and Pavement Design 4(1), 77–107.
6. Francken, L., & Verstraeten, J. (1975). Relation entre le module de rigidité d'un enrobé bitumineux et le module de cisaillement du bitume qu'il renferme. Rapport du deuxième colloque international rilem consacré aux essais sur bitumes et matériaux bitumineux, Budapest (Vol. 1, pp. 375–388).
7. Francken, L. (1977). Module complexe des mélanges bitumineux. Bulletin de liaison des laboratoires des ponts et chaussées, Spécial V, 181–198.
8. Huet, Ch. (1963). Étude par méthode d'impédance du comportement viscoélastique des matériaux hydrocarbonés. Thèse du grade d'ingenieur-docteur (140 p.). Paris.
9. Sayegh, G. (1965). Contribution à l'Étude des Propriétés Viscoélastiques de Bitumes Purs et des Bétons Bitumineux. Thèse du docteur – ingénieur (133 p.). Paris.
10. Bahia, H.V., Zhai, H., Bonetti, K., & Kose, S. (1999). Non-linear viscoelastic and fatigue properties of asphalt binders. Association of Asphalt Paving Technologists, 68, 1–35.
11. Airey, G.D., Rahimzadeh, B., & Collop, A.C. (2011). Linear Viscoelastic Performance of Asphaltic Materials. Road Materials and Pavement Design, Volume 4, Issue 3, (pp. 269–292). https://doi.org/10.1080/14680629.2003.9689949.
12. Liao, Min-Chih, Chen, Jian-Shiuh & Airey Gordon (2015). Characterization of Viscoelastic Properties of Bitumen-Filler

Mastics, Asian Transport Studies, Volume 3, Issue 3, (pp.312-32).
13. Babadopulos, L., Orozco, G., Mangiafico, S., Sauzéat, C. & Di Benedetto, H. (2019) Influence of loading amplitude on viscoelastic properties of bitumen, mastic and bituminous mixtures, Road Materials and Pavement Design, 20:sup2, S780-S796, DOI: 10.1080/14680629.2019.1628428.
14. Zolotarev, V., Pyrig, Y., & Galkin, A. (2018). Cohesion of bitumen: its opportunities and prospects. Road Materials and Pavement Design. doi: 10.1080/14680629.2018.1551149.
15. EN 12697-26:2012 (2018). Bituminous mixtures. Test methods. Stiffness. European Committee for Standardization.
16. Лапченко, А.С. (2010). Реологические свойства асфальтополимербетонов при динамическом деформировании. Ph.D. thesis (231 p.). Kharkov.
17. Золотарёв В.А. Разгаданная пенетрация. Наука и Техника в Дорожной отрасли №4, 2018. с 38-40.
18. Руденский А.В., Руденская И.М. Реологические свойства битумных смесей. М.: «Высшая Школа». -1971. -131 с.
19. Molenaar, J.M.M., Hagos, E.T., Van de Ven, M.F.C., & Hofman, R. (2004). An investigation into the analysis of polymer modified asphalt. Proceedings of 3rd Eurasphalt & Eurobitume Congress, Vienna (Paper 203, Book II, pp. 2080–2091).
20. Isayev, A., Zolotarev, V.A., & Vinogradov, G.V. (1975). Viscoelastic properties of bitumens in continuous and cyclic deformation. Rheologica Acta 14, 135–144.
21. Des Croix, P., & Di Benedetto, H. (1996). Binder-mix rheology: limits of linear domain, non linear behavior. Eurasphalt & Eurobitume Congress, Strasbourg (Vol. 2, Paper E&E.5.107).
22. Chappat, M., & Ferraro, M. (1997). Pour y voir clair dans les essais SHRP et dans leur application aux bitumes polymères. Revue générale des routes et aérodromes, 753, 47–55.
23. Vinogradov, G.V., Isayev, A.I, Zolotarev, V.A., & Verebskaya, E.A. (1977). Rheological properties of paving bitumen. Rheologica Acta 16, 266–281.
24. Радовский Б.С., Телтаев Б.Б., Вязкоупругие характеристики битумов и их оценка по стандартным показателям. Алматы «Білім Баспасы». –2013. –152с.
25. Goacolou, H., & Mazé, M. (2000). Enrobés à haut module élastique. Proceedings of the Papers Submitted for Review. 2nd Eurasphalt–Eurobitume Congress. Barcelona (Book 1, pp. 269–275).
26. De la Roche, Ch., Di Benedetto, H., & Doubbaneh, E. (1999). Fiabilité des essais de module complex sur enrobés. Comparaison d'essais en flexion et en traction–compression. Eurobitume Workshop 99 (Paper 31).
27. Buttlar, W.G., & Al –Khateeb, G.G. (2003). Evaluating creep compliance of asphaltic paving mixtures using a hollow-cylinder tensile tester. Proceedings of the 6h International RILEM Symposium (pp. 527–533).
28. Olard, F., Noel, F., & Loup, F. (2005). Mesure du module diamétrale des enrobés bitumineux. Revue générale des routes et aérodromes, 844, 77–83.

The Generators Created by Ferranti and Hasselwander, a Subject to Study to Save on Current Electrical Energy Production

Pedro O. Diaz, & Orestes Hernández

University of Havana

ABSTRACT

The electromagnetic torque, antagonistic to the movement that to prime mover exerts on the shaft the contemporary synchronous generator, it is the fundamental cause of the enormous amount of energy consumed in thermoelectric plants, diesel - generators, hydroelectric plants, wind turbines, etc.; in this text, two old alternators from the 19th century are analyzed: Ferranti and Hasselwander, great British and German engineers respectively, while this text mentions about the homopolar generator, all today seen as museum objects due to their great historical value, however their behavior with respect to the harmful electromagnetic torque is much lower than in the current synchronous generator; based on the study of both electric generators, it is demonstrable that by modifying the magnetic circuit of the current synchronous generator it is possible to generate with less electromagnetic torque, which is equivalent, assuming constant rotation speed, to lower power consumption in the primary motor only by changing the magnetic circuit of the generator.

Keywords: synchronous generator torque, primary energy saving.

Classification: DDC Code: E LCC Code: KF26

Language: English

London Journals Press

LJP Copyright ID: 392954
Print ISSN: 2631-8474
Online ISSN: 2631-8482

London Journal of Engineering Research

Volume 22 | Issue 9 | Compilation 1.0

The Generators Created by Ferranti and Hasselwander, a Subject to Study to Save on Current Electrical Energy Production

Pedro O. Diaz[α] & Orestes Hernández[σ]

ABSTRACT

The electromagnetic torque, antagonistic to the movement that to prime mover exerts on the shaft the contemporary synchronous generator, it is the fundamental cause of the enormous amount of energy consumed in thermoelectric plants, diesel - generators, hydroelectric plants, wind turbines, etc.; in this text, two old alternators from the 19th century are analyzed: Ferranti and Hasselwander, great British and German engineers respectively, while this text mentions about the homopolar generator, all today seen as museum objects due to their great historical value, however their behavior with respect to the harmful electromagnetic torque is much lower than in the current synchronous generator; based on the study of both electric generators, it is demonstrable that by modifying the magnetic circuit of the current synchronous generator it is possible to generate with less electromagnetic torque, which is equivalent, assuming constant rotation speed, to lower power consumption in the primary motor only by changing the magnetic circuit of the generator.

Keywords: synchronous generator torque, primary energy saving.

Author α: Pedro Osvaldo Díaz Fustier, Electric Engineer, Master in Sciences, Technological University of Havana, Faculty of Electrical Engineering, Electroenergetic Testing and Research Center, Havana, Cuba.

σ: Orestes Hernandez Areu, Electric Engineer, Doctor in Sciences, Director Electroenergetic Testing and Research Center, Technological University of Havana, Faculty of Electrical Engineering, Electroenergetic Testing and Research Center, Havana, Cuba.

I. INTRODUCTION

When electrical machines are studied today, the synchronous motor and the synchronous generator are practically very similar, however at the beginning of the 20th century several types of generators were successfully serving, but the design of Siemens was imposed technologically, leaving the vast majority as museum objects the other designs, the constructive feasibility and a very high efficiency make generators and synchronous motors today practically the same machine, protected by the Principle of Reversibility of Electrical Machines.

The very high efficiency of the current synchronous generator makes us believe that it is absurd to look for primary energy savings by modifying something of proven excellence and it would be very true scientifically to look for more efficiency by minimizing losses, which is already something very successful today technologically, large commercial synchronous generators exceed the 98% efficiency and even 99%, minimizing energy losses.

Among the set of energy losses of a synchronous generator, the antagonistic electromagnetic torque to the mechanical torque injected into the shaft is not counted as such, but it is consuming primary energy (renewable or not), brakes proportional to the load connected to its output, this brake is compensated with more primary power; although this phenomenon is inevitable, it is possible to minimize it.

At the beginning of the 20th century, energy consumption was not seen with the strategic and environmental importance it has today, it was not the amount of electrical energy required today

necessary, and fuel costs were low, for all of which it lacked technical - economical importance the electromagnetic torque Vs the production cost and versatility of the Siemens generator commercially in use today.

The generators that present less antagonistic torque with connected load are:

- Homopolar generator
- Ferranti generator
- Hasselwander generator

As is known, none of these electric generators is used commercially today.

II. THE CURRENT CONTEXT

Today's synchronous generator is a much more technologically developed form of the synchronous generator designed by Siemens in the 19th century.

In a synchronous generator, when delivering power to a given load, there is a group of energy *losses:*

- Mechanical losses.
- I2R thermal losses.
- Losses due to parasitic currents.
- Additional losses.
- Magnetic losses due to dispersion.

A worthy example of the high efficiency achieved in minimizing the afore mentioned losses in synchronous generators is the Siemens SGen 2000P Series from 370MVA to 560MVA, which achieves efficiency above 99% [6].

Considering that the rotation speed of a synchronous generator is constant, the primary power consumption depends on the antagonistic torque exerted on its shaft, which is the electromagnetic torque exerted between the rotor and the stator, it is what determines the necessary mechanical power consumption at each moment, all of which is expressed as follows:

$$P_{Mec} = \omega T_{Total} \quad (1)$$

Being ω constant, the mechanical power consumption is a function of the torque,

$$T_{Total} = J_{Rotor}\omega + T_{friction} + T_{EM} \quad (2)$$

$$J_{Rotor} = mr^2 \quad (3)$$

Where J_{rotor} ω is the inertial torque [7] of the rotor, $T_{friction}$ is the frictional torque of the rotor and T_{EM} is the antagonistic torque exerted on the shaft due to its main magnetic circuit and the electric current it supplies to the load, called electromagnetic torque, the latter much greater quantitatively, that is why most of the mechanical power supplied to the shaft is consumed in overcoming this harmful torque, antagonistic to motor movement

III. THE ELECTROMAGNETIC TORQUE IN THE SYNCHRONOUS GENERATOR

The electromagnetic torque in rotating electrical machines is the interaction between the forces exerted rotor - stator, with a positive direction in electric motors, but negative or antagonistic in the specific case of the synchronous generator (Fig. 1), in both machines referred to the interaction between static and rotating magnetic fields.

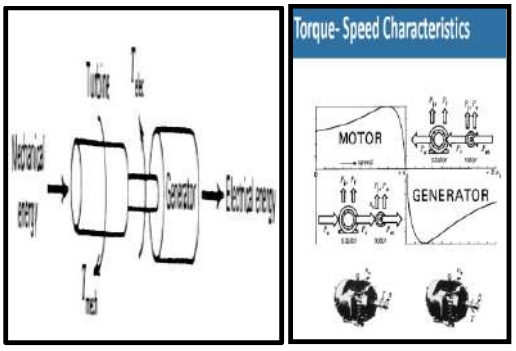

Fig. 1: The Electromagnetic Torque in the Synchronous Generator

The existing magnetic fields in the stator and rotor of the synchronous generator interact based on the mutual inductances
[8].

The mutual inductance $M_{R\leftarrow S}$ of the induced winding with respect to the field winding is the ratio of the magnetic flux through the N_R turns of the induced winding produced by the magnetic field of the current I_S through the field winding, that is:

$$\mathbf{M_{R\leftarrow S}} = \frac{\mathbf{N_R \Phi_{R\leftarrow S}}}{\mathbf{I_S}} = \frac{\mathbf{N_R(B_S \times (A_S))}}{\mathbf{I_S}} \quad \textbf{(4)}$$

$$\mathbf{M_{R\leftarrow S}} = \frac{\mu_0 \mu_{rel} N_R A_S}{\ell_S} \quad \textbf{(5)}$$

While the mutual inductance $M_{S\leftarrow R}$ of the field winding with respect to the induced winding is the ratio of the magnetic flux through the N_S turns of the field winding produced by the magnetic field of the I_R current through the induced winding, that is:

$$\mathbf{M_{S\leftarrow R}} = \frac{\mathbf{N_S \Phi_{S\leftarrow R}}}{\mathbf{I_R}} = \frac{\mathbf{N_S(B_R \times (A_R))}}{\mathbf{I_R}} \quad \textbf{(6)}$$

$$\mathbf{M_{S\leftarrow R}} = \frac{\mu_0 N_R A_R}{\ell_R} \quad \textbf{(7)}$$

for all of which the equivalent mutual inductance will be:

$$M = \begin{vmatrix} L_{Rotor} & M_{R\to S} \\ M_{S\to R} & L_{Stator} \end{vmatrix} \quad \textbf{(8)}$$

$$M = L_{Rotor} L_{Stator} - M_{R\to S}(M_{S\to R}) \quad \textbf{(9)}$$

The torque equation in a three-phase commercial synchronous machine [9] stated as a function of mutual inductance is:

$$T = -pMif\,(ia\overset{R}{S}en(p\varnothing) + ibSen\,(p\varnothing - 2\pi) + i\,Sen\,(p\varnothing + 2\pi)) \quad (10)$$

There are other methods of evaluating the electromagnetic torque, based on Park's equations [10] and it is expressed as:

$$T = i_q \Psi_d - i_d \Psi_q = i_q(i_d L_d) - i_d\,(i_q L_q) \quad (11)$$

Where $iq\Psi d - id\Psi q$ is a difference between vector products and flux linkages $\Psi = L_i$. The electromagnetic torque equation in a three-phase synchronous generator as a function of the magneto-motive forces (M.M.F) is:

$$T_{EM} = k.\bar{B}_{Stator}.\bar{B}_{Rotor}.Sin(\delta) \quad \textbf{(12)}$$

$$T_{EM} = k.(\overline{MMF}_{Stator}).(\overline{MMF}_{Rotor})Sin(\delta) \quad \textbf{(13)}$$

Once the basic issues on the subject have been expressed, each of the three types of electric generators with less electromagnetic torque will be analyze, to apply to the current electro-energy context in search of primary energy savings.

VI. THE HOMOPOLAR GENERATOR IN THE CURRENT CONTEXT

The homopolar generator (Fig. 2) is a direct current machine initially designed by Michael Faraday in 1831, consisting of a disc of electrically conductive material, rotating in a magnetic field perpendicular to it, where the energy is extracted between the edges of the disc and its center.

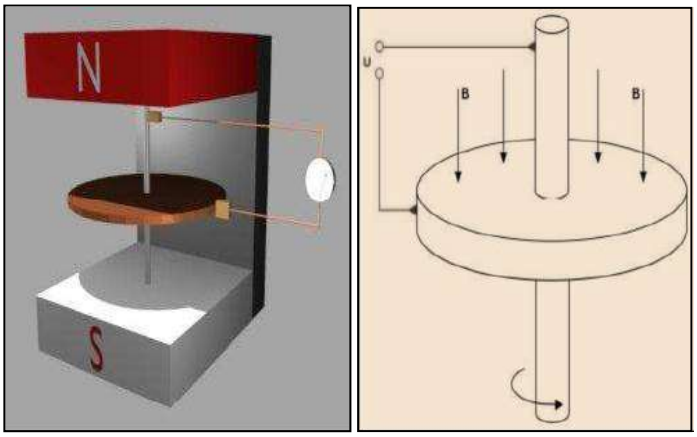

Fig. 2: Basic Homopolar Generator

It is characterized by very low voltage and very high current, a very pure direct current, the interaction between rotor and stator is very low despite the very high current values with which it is capable of contributing to the load.

This small relationship between the current and the antagonistic torque that this generator produces was exposed in Germany in September 2016, the German Electrical Union and the Swiss Electrical Union sponsored a great event in the Congress Center of Wurzburg, [11] Germany, where the Indian scientist Tewari defended his modification to the homopolar generator (Fig. 3), unfortunately despite the successful result, the physical argument is not scientifically validated because an absurd disproportion between the input and output energies is affirmed, although the low torque antagonistic is logical and probable.

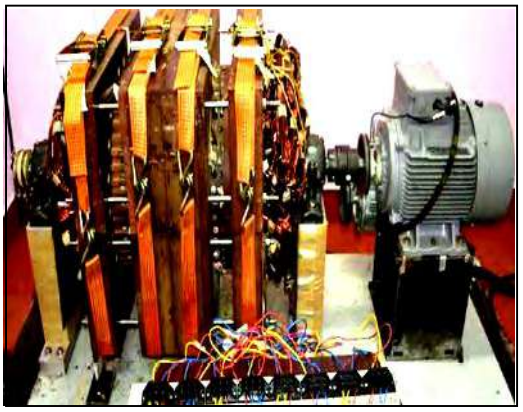

Fig. 3: Homopolar Generator Exhibited by Indian Scientist Paramhamsa Tewari at Conference in Würzburg, Germany in 2016

The homopolar generator continues to be scientifically investigated today.

V. THE FERRANTI GENERATOR IN THE CURRENT CONTEXT

The alternator designed by Zianni Ferranti (1864 – 1930) had an inductor with a ferromagnetic core and an induced core with an air core, axial magnetic flux and exciter mounted on the shaft, specifically in Fig.4 it can be seen that each 1MW synchronous generator is moved by 1500 HP (1.12MW) machines with approximately 89.4% efficiency, excellent for those times.

Given his personal friendship with Siemens and the economic superiority of the radial magnetic flux synchronous generator model proposed by his German colleague, which in turn also allowed the material to be used to build motors, Ferranti abandoned continuing to perfect his inventiveness, collaborating with Siemens on his technology, it still existing today.

Fig. 4: Ferranti Alternator: First Thermoelectric Plant in the World (Deptford Station, London, Great Britain, 1889), Whose 1MW Synchronous Generators Were Designed by Zianni Ferranti

In the Electrical Machines Laboratory of the Technological University of Havana, successful tests were carried out (2004) with a design based on the old Ferranti generator (Fig. 5), but seeking to save primary energy [12] based on the lower antagonistic torque it presents.

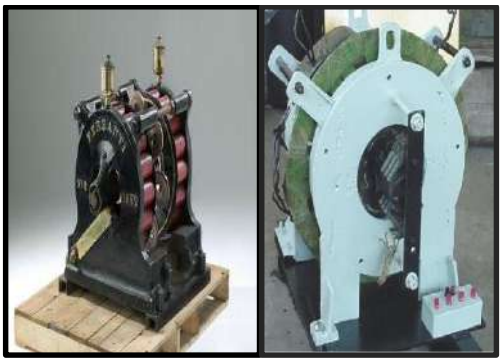

Fig. 5: Left: Ferranti generator (United Kingdom, 1882). Right: Low reversibility electric generator (Cuba, 2004)

There are 2 classic ways (there is a third: deforming the core) to vary the magnetic flux: varying the electric current (for example, the transformer) or varying it mechanically (for example, in electric generators); in both cases the electrical energy is produced in a unidirectional action: inductor to induced; once produced, the delivery of that electrical energy to perform work on the connected load creates a series of electrical, magnetic and mechanical losses, but

fundamentally reflected in the presence of the electromagnetic torque resistant to rotation injected by the prime mover, main concern in this text due to the high cost of primary energy and the growing need for electrical energy.

Fig. 6: Low Reversibility Electric Generator (2004), on the Right Its Rotor

Constructively (Fig. 6) the low reversibility electric generator consists of a stator completely lacking in lamination, made of carbon steel (C20 and C45), 4 poles wound with AWG 15 wire, while the rotor consists of 3 windings at 120° offset from each other, with 4 poles each, rectangular wire (2.00 x 2.80 mm), the output is through 3 sliding rings (12.5kVA / 10kW / 230V, three-phase).

The calculation of its relative parameters is as follows:

$$\mathbf{Z_b = \frac{U_f}{I_f} = \frac{230V/\sqrt{3}}{31{,}8A} = 4{,}18\ ohm} \quad \textbf{(14)}$$

$$\mathbf{X_{dp.u} = \frac{X_d}{Z_b} = \frac{2{,}17}{4{,}18} = 0{,}519} \quad \textbf{(15)}$$

$$\mathbf{X_{qp.u} = \frac{X_q}{Z_b} = \frac{1{,}32}{4{,}18} = 0{,}316} \quad \textbf{(16)}$$

Being its Short Circuit Ratio the following:

$$\mathbf{\frac{1}{X_d} = 1{,}93} \quad \textbf{(17)}$$

Table 1: Experimental Calculation of Efficiency in Low Reversibility Electric Generator 12.5kVA, 10 kW, Cos ϕ = 0,8 Ind, 4 Poles, 1500rpm Constant

Nominal Power	***10 kW***
Seem Power	***12,5 kVA***
Mechanical losses	***0,32 kW***
Steel losses	***View not***
Cooper losses	***1,21 kW***
Other losses	***0,055 kW***
Total losses	***1,585 kW***
Efficiency	***86,32%***

Table 2: Comparative Table Between Current Commercial Generators [13, 14 Y 15] and the Low Reversibility Electric Generator at the Same Rated Power, Number of Poles and Rotation Speed

Potencia 100 % / 0,8 ind.	Stamford 2004	Stamford 2019	Low reversibility	Leroy Somer 2020
V_{nom}	230 / 115 Volt	380 / 220 Volt	230 / 127 Volt	230 / 115 Volt
S_{nom}	12,5 kVA	12,5 kVA	12,5 kVA	12 kVA
Cos φ	0,8 inductivo	0,8 inductivo	0,8 inductivo	0,8 inductivo
P_{nom}	10 kW	10 kW	10 kW	10,2 kW
Eficiencia	78%	81,50%	86,32%	84,4 % (FP=!)
Relación Corto Circuito	0,495	0,493	1,927	No dato
Xd (p.u)	2,02	2,03	0,519	No dato
Xq (p.u)	1,01	0,98	0,316	No dato
Paso Polar	Dos tercios	Dos tercios	1	Dos tercios
Flujo Magnético	Radial	Radial	Axial	Radial

Tables 1 and 2 show the prospects for developing this construction technology of the synchronous generator, because despite the obvious technical shortcomings with which the project was developed, there is approximately 5% better energy efficiency.

VI. THE HASSELWANDER GENERATOR IN THE CURRENT CONTEXT

The German engineer Friedrich August Hasselwander is credited as the author of the first three-phase synchronous generator (Fig. 7), this produced 2.8 kW, 4 poles, 960 rpm (32 Hz), and this generator was presented at the Frankfurt exhibition of 1891.

In 2020 an experiment was carried out to study the physical behavior of the Hasselwander generator at our university, for which there was a lack of a toroid with

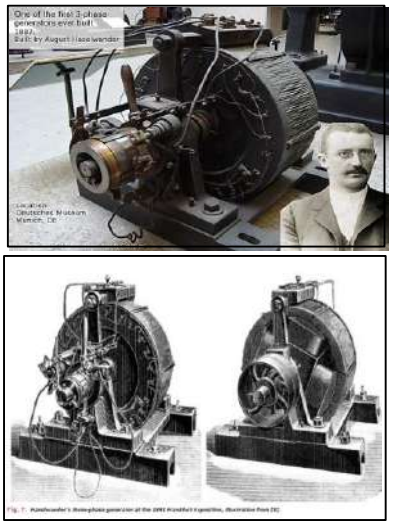

Fig. 7: Synchronous Generator Hasselwander: First Three-Phase Generator in the History

core had lamination in the direction convenient to the rotation of the inductor, for which a square transformer core was taken (Fig. 8), this results in the magnetic flux emanating from the rotor having additional dispersion losses, in addition of an excessive air gap.

Fig. 8: Experiment to Study Electromagnetic Torque in a Hasselwander Generator. Above: Side and Diagonal View. Below: The Rotor - Stator Assembly in a Demonstration Photo of Physical Layout

The behavior of the project is compared with a commercial alternator of 120 Watt power at 1800 rpm (Fig. 9), in the event of a controlled short circuit.

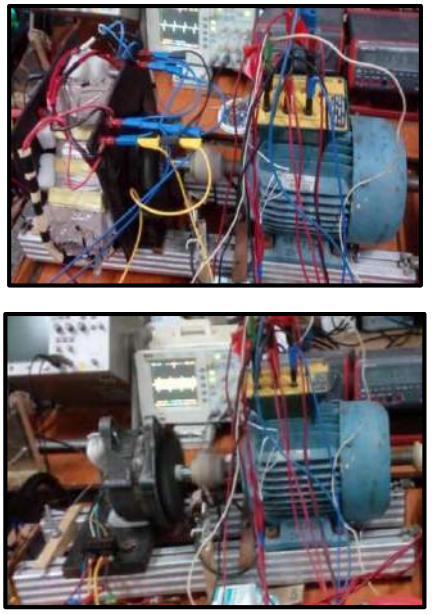

Fig. 9: Comparison before a controlled short circuit of a commercial generator Vs experimental generator. Above: With experimental generator. Below: With classic generator

The experiment presented the result shown in table 3.

Table 3: Comparative table of antagonistic torque and mechanical power of the LADA AAG (120W) automobile alternator and a rudimentary experimental generator in the event of a stable 18 Amp short circuit presented to the Scientific Council of the Faculty of Electrical Engineering (CIPEL / CUJAE) in 2020

*Not load: LADA I_{EXC} nominal = 2,5 A GSBR I_{EXC} = 12 A	NOT LOAD*	SHORT CIRCUIT OF 18 A
Mechanical power in the shaft of the synchronous generator LADA AAG (w)	109,03	213,63
Torque in the shaft of the synchronous generator LADA AAG (N-m)	0,58	1,139
Mechanical power in the shaft of the experimental synchronous generator (w)	18	71,88
Torque in the shaft of the proposed synchronous generator (N-m)	0,095	0,382

The table 3 shows the enormous torque difference in the prime mover at the same controlled short-circuit current value (18Amp) existing between both generators.

VII. CONCLUSIONS

In any of the 3 generators mentioned in this text, it is observed that the electromagnetic torque is less than its current commercial counterpart; of course, in all cases, it is necessary to perfect the disadvantages that they present and find the design of an only synchronous generator that optimizes the consumption of primary energy.

Saving in a technologically accessible future, for example, 10% of primary energy by changing the magnetic circuit of the current synchronous generator would bring in generator sets, whose internal combustion engine generally does not reach 40% efficiency, savings of perhaps 20% in fuel consumption, in wind energy limited by the Betz constant, would allow the diameter of the blades to be reduced to deliver similar power; it is not possible to speak of exact savings numbers because they are non-linear processes.

In addition, which is also very important, it would allow sustainable savings because modifying the electric generator does not harm the environment and would take advantage of all the existing infrastructure today.

REFERENCES

1. Litvin D. B., One-piece Faraday generator: A paradoxical experiment from 1851, https://www.researchgate.net/publication/258890379, DOI: 10.1119/1.11109, American Journal of Physics , U.S.A, July 1978.
2. Montgomery H., Unipolar induction: a neglected topic in the teaching of electromagnetism, Eur. J. Phys. 20 (1999) 271–280, PII: S0143-0807(99)99918-X. U.K, 1999.
3. Baymani M., Study of Homopolar DC Generator, thesis for the degree of Doctor of Philosophy in the Faculty of Engineering and Physical Sciences, University of Manchester, U.K, 2012.
4. Brain, Robert, Sebastian Zianni de Ferranti, Pioneer of Electric Power, https://www.google.com/url?sa=t&rct=j&q=&esrc=s&source=web&cd=&cad=rja&uact=8&ved=2ahUKEwjPlvzzzZX7AhXxTDABHTeXBZYQFnoECQAQ&url=http%3A%2F%2Fwww.hevac-heritage.org%2Fbuilt_environment%2Fpioneers_revisited%2Fsurnames_a-o%2Fferranti.pdf&usg=AOvVaw1 5MWUmaxOcnCnavud9LuDy.
5. Hooshyar H, Synchronous generator: Past, present and future, October 2007, DOI: 10.1109/AFRCON.2007.4401482, https://www.google.com/url?sa=t&rct=j&q=&esrc=s&source=web&cd=&cad=rja&uact=8&ved=2ahUKEwibu-mby5X7AhX1czABHal2DuUQFnoECA0QAQ&url=https%3A%2F%2Fwww.researchgate.net%2Ffigure%2FThe-first-three-phase-synchronous-machine-built-by-Friedrich-August-Haselwander-in-1887_fig1_4297837&usg=AOvVa w2x2G1AAuACG-V6ku12TsSz.
6. Synchronus generator Siemens Serie SGen 2000P 370MVA to 560MVA https://www.google.com/url?sa=t&rct=j&q=&esrc=s&source=web&cd=&cad=rja&uact=8&ved=2ahUKEwjSuOC715X7AhVXSTABHaMYD0IQFnoECA4QAQ&url=https%3 A%2F%2Fwww.siemens-energy.com%2Fglobal%2Fen%2Fofferings%2Fpower- generation%2Fgenerators%2Fsgen-2000p.html&usg=AOvVaw1EXHlWl2mR4w6iYWdfCHx-
7. Morgan, K., Torque and angular momentum in circular motion, Project PHYSNET Physics Bldg. Michigan State University East Lansing, MI 48824; (517) 355- 3784, http://www.physnet.org/home/mod ules/license.html.
8. Silvester S., Electricidad y magnétismo, Inducción magnética, https://www.google.com/url?sa=t&rct=j&q=&esrc=s&source=web&cd=&cad=rja&uact=8&ved=2ahUKE wjBj-va5Jn7AhVkVTABHSfDBY4QFnoECA4QAQ&url=http%3A%2F%2Fwww.fisica.edu.uy%2F~cris%2F teaching%2Fmasoller_AF_tema6.pdf&usg=AOvVaw1WJu51azleVvD m9951spzv.
9. Lipo, T. A., Synchronous machines, Chapter 3 The d–q Equations of a Synchronous Machine, Taylor & Francis Group, LLC CRC,International Standard Book Number-13: 978-1-4398-8068-5 (eBook - PDF), 2012, Estados Unidos.
10. R.H. Park, Two-Reaction Theory of Synchronous Machines, Generalized Method of Analysis— Part I, Trans. of the AIEE, 1929, pp. 716–730, 1929, Estados Unidos.

11. Defense Forum India, India permits free energy technology, 2016 https://www. google.com/url?sa=t&rct=j&q=&esrc=s&source=web&cd =&cad=rja&uact=8&ved=2ahUKEwiBmcf4_5n7AhUASTABHR2bB50QFnoECAwQAQ&url=https%3A%2F%2Fdefenceforumindia.com %2Fthreads%2Findia-permits-free-energy-technology.77713%2F&usg=AOvVaw1jiX6fdn5mfsGT85jhbC1v
12. Diaz F, Pedro O., Generador sincrónico de baja reversibilidad, Tesis de Máster en Ciencias, Laboratorio Máquinas Eléctricas, Universidad Tecnológica de la Habana, 2004, Habana, Cuba.
13. Stamford Power Generation, PI 042D Technical data sheet, Reino Unido, 2004.
14. Stamford PI044F 2019- Winding 311 https://www.stamford- avk.com/stamford-avk/sites/stamfordavk/files/PI044F-311-TD-EN_Rev_A.pdf.
15. Low Voltage Alternator - 4 pole, Dedicated single phase, 10.5 to 16 kVA - 50 Hz / 11.5 to 17.5 kVA - 60 Hz, Electrical and mechanical data, Leroy Somer Series LSA 40, http:// www.leroy-somer.com/epg, March 2020.